JBC RESEARCH ARTICLE

HIF-2α induction in *de novo* lipogenesis in metabolic dysfunction-associated steatohepatitis is dependent on IL-21 signaling

Received for publication, October 15, 2025, and in revised form, January 6, 2026 Published, Papers in Press, January 29, 2026
https://doi.org/10.1016/j.jbc.2026.111212

Karla K. Frietze[1], Alyssa Brown[1], Dividutta Das[1], Raymond Franks[1], Pranavi Jagadeesan[1], and Joseph T. Nickels Jr[1,2,*]

From the [1]The Institute of Metabolic Disorders, Genesis Biotechnology Group, Hamilton, New Jersey, USA; and [2]Rutgers Center for Lipid Research, New Jersey Institute for Food, Nutrition, and Health, Rutgers University, New Brunswick, New Jersey, USA

Reviewed by members of the JBC Editorial Board. Edited by Qi-Qun Tang

The prevalence of metabolic dysfunction-associated steatotic liver disease (MASLD) and metabolic dysfunction-associated steatohepatitis (MASH) has reached epidemic proportions globally. Understanding the molecular mechanisms that underlie these conditions offers significant potential for identifying new therapeutic targets. In this study, interleukin-21 receptor-deficient mice were used to investigate the role of IL-21 signaling in obesity-induced MASLD and MASH. Findings reveal that *IL21R*$^{+/+}$ mice exposed to a high-fat diet develop MASLD/MASH, with hepatic activation of IL-21 signaling driving *de novo* lipogenesis through Janus kinase 1-STAT5-dependent induction of hypoxia-induced transcription factor 2α (HIF-2α). HIF-2α elevation stimulates genes involved in *de novo* lipogenesis, contributing to increased hepatic lipid accumulation and MASLD progression. Elevated levels of TGF-β1 and increased collagen deposition indicate hepatic stellate cell activation, facilitating the development of liver fibrosis. Moreover, upregulation of HIF-2α enhances expression of the amino acid transporter solute carrier family 7 member 5, leading to mammalian target of rapamycin complex 1-mediated inhibition of autophagy. In contrast, *il21r*$^{-/-}$ mice exhibited diminished Janus kinase 1-STAT5 signaling and were protected from MASLD/MASH. Liver from individuals afflicted with fatty liver disease or nodular cirrhosis show increased IL-21R protein that co-localized with CD4, implicating activated T cells as a potential source of IL-21 for receptor activation. Collectively, these results indicate that targeting IL-21 receptor signaling may represent a promising strategy for reducing MASLD/MASH.

The global rise in obesity is associated with an increased prevalence of metabolic dysfunction-associated steatotic fatty liver disease (MASLD) and metabolic dysfunction-associated steatohepatitis (MASH) (1, 2). Approximately 40% of the world's population has obesity, and around 70% of these individuals are affected by MASLD (3). Health care costs related to these conditions are estimated at $150 billion dollars per year and are projected to rapidly increase over the next 10 years (4). Rezdiffra, a thyroid hormone receptor-β agonist, and is currently being used to treat individuals with MASLD (5) and clinical evidence indicates its utility as a treatment for MASH (6). Clinical trial data has also suggested that glucagon-like peptide-1 receptor agonists, such as semaglutide, may also be effective options, and Wegovy has recently received FDA approval for the treatment of MASH (7). However, these medications are associated with certain side effects (8, 9), and research into alternative and/or adjunct therapies is ongoing and active (10).

Interleukin-21 (IL-21) receptor (IL-21R), a type I cytokine receptor produced by T cells and natural killer T cells, binds to the IL-21R-γ chain complex to initiate IL-21 signaling (11, 12). Mutations in the common γ chain are associated with X-linked severe combined immunodeficiency caused by defective IL-21 signaling (13). IL-21 receptor binding initiates the Janus kinase (JAK)-STAT signaling cascade, resulting in phosphorylation of the STAT1, STAT3, and STAT5 transcription factors, which modulate T and B cell differentiation, apoptosis, and IL-10 production (14). Additionally, IL-21 engages the phosphatidylinositol 3-kinase and MAPK pathways to control cell proliferation, apoptosis, and survival (14). STAT3 is primarily responsible for IL-21R signal transduction (15). Both STAT1 and STAT3 can modulate IL-21R signaling through their opposing actions on downstream receptor signals (16). The biological relevance of STAT5 activation, particularly in relation to JAK-dependent transcriptional regulation, is not yet well established.

IL-21R signaling has been strongly associated with liver injury (17–19). IL-21R expression is elevated in the liver of patients diagnosed with hepatocellular carcinoma, and increased *IL-21R* levels have been correlated with reduced survival rates (17). Higher expression is also apparent in several inflammatory liver disorders, including primary biliary cholangitis and parasitic infections (20, 21). IL-21R signaling promotes the induction of interferon γ, which plays a role in the advancement of hepatic inflammation during MASH through activation of Toll-like receptor 2 pathways (22). Additionally, IL-21 facilitates hepatitis B-related liver cirrhosis by stimulating hepatic stellate cells (23), a process implicated in fibrosis observed in MASH (24).

* For correspondence: Joseph T. Nickels, jnickels@mdlab.com, Jr.

il-21r$^{-/-}$ *mice are resistant to MASLD/MASH*

Clinical studies have shown that MASLD may advance more rapidly in individuals who have obstructive sleep apnea and are exposed to chronic intermittent hypoxia (25–27). Studies using animal models indicate that mice exposed to chronic intermittent hypoxia show increased susceptibility to oxidative damage and inflammation in the liver (28, 29). Livers with MASLD/MASH are exposed to hypoxic conditions, which can lead to inflammation, lipid accumulation, and fibrosis (30). Hypoxia-induced transcription factor signaling, like that seen for hypoxia-induced factor (HIF)-2α, is elevated in MASH and linked to fibrosis (31). Their target genes include those involved in fatty acid and cholesterol biosynthesis (32).

IL-21R expression has been reported to increase under hypoxic conditions in a hindlimb ischemia mouse model for peripheral arterial disease (33), while TNF, IL-1, and IL-6, have been reported to be elevated in hypoxic liver (34). Studies have shown that *tnfr*$^{-/-}$ mice do not develop MASH (35), and a similar resistance is observed in mice lacking IL-6 (36). Therefore, it is possible that IL-21R signaling is activated under hypoxic conditions and contributes to the pathogenesis of MASLD/MASH.

Our previous study showed that the overexpression of retinoic acid-inducible gene-I (RIG-I) mitigates lipotoxic steatotic conditions in HepG2 cells (37). In addition, reduced RIG-I levels were observed in mice subjected to a steatotic diet. In this study, mRNA transcriptomic analysis identified IL-21R as one of six genes differentially regulated by RIG-I gene dosage under lipotoxic conditions in HepG2 cells. Building upon these findings, we investigated the function of IL-21R signaling in MASLD/MASH using *Il-21r*$^{-/-}$ knockout mice. Our data demonstrate that IL-21R signaling promotes MASH progression by activating the JAK1-STAT5 pathway, which subsequently drives lipogenesis mediated by the hypoxia-inducible transcription factor HIF-2α. Furthermore, JAK1-STAT5 exacerbates MASH by activating mammalian target of rapamycin complex 1 (mTORC1), thereby inhibiting autophagy.

Results

IL-21R *expression is elevated in steatotic HepG2 cells*

Previously, we found that palmitic acid (PA) treatment lowered RIG-I levels in HepG2 cells, RIG-I overexpression reduced lipotoxic cell death, and mice on a steatotic diet showed decreased RIG-I protein (37). To examine the potential effects of RIG-I overexpression on lipotoxicity, HepG2 cells with either increased or reduced RIG-I expression were treated with PA. mRNA transcriptomic analysis was conducted to identify genes whose expression was changed because of different levels of RIG-I.

Genes associated with RIG-I dosage were identified by RNASeq analysis as being differentially upregulated in PA-treated cells; their expression increased further in PA-treated cells with RIG-I knockdown and decreased in PA-treated cells with RIG-I overexpression (Fig. S1*A*). Of those, *DDIT3* (*CHOP*), C-X-C motif chemokine ligand 8, *IL-21R*, *CXCL2*, *NEURL3*, and tumor necrosis family receptor super family 9 (*TNFRSF9*), were identified under all conditions (Fig. S1*B*). Elevated gene expression in PA-treated HepG2 cells was confirmed by quantitative reverse transcription-polymerase chain reaction (*q*RT-PCR), except for *CXCl2* and *NEURL3* (Fig. S1*C*).

DDIT3 (CHOP) is an ER stress-activated transcription factor involved in the unfolded protein response and has been associated with MASH progression (38). The cytokine C-X-C motif chemokine ligand 8 (IL-8) attracts neutrophils, monocytes, and macrophages to inflamed liver sites during MASH (39). TNFRSF9 is part of the TNF receptor family (40), and Mendelian randomization studies have shown a causal link between MASLD and increased *TNFRSF9* expression (41).

Increased IL-21R expression has been observed in the liver of individuals diagnosed with MASH-associated hepatocellular carcinoma (17). Given the feasibility of high throughput screening of the target genes identified, we decided to focus our studies on the role of IL-21R signaling in MASLD/MASH to test its therapeutic potential.

Il-21r$^{-/-}$ *mice become obese on a high-fat diet*

IL-21R$^{+/+}$ and *il-21r*$^{-/-}$ mice were administered a 60% high-fat diet (HFD) for 16 weeks, with body weights and food intake measured on designated days. A small but statistically significant difference in body weight gain was observed between the cohorts; notably, *il-21r*$^{-/-}$ mice exhibited reduced weight gain regardless of dietary regimen (Fig. 1*A*; chow, 8%; HFD, 7%), as seen by decreases in AUC values (Fig. 1*B*; blue bars *vs.* purple bars). Food consumption results showed that *il-21r*$^{-/-}$ mice ate less of both diets (Fig. 1*C*; chow, 15%; HFD, 6%). Notably, both cohorts consumed less of the HFD compared to chow (Fig. 2*D*). Overall, chow-fed *il-21r*$^{-/-}$ mice gained less weight and consumed less food. As they showed no signs of illness, IL-21R signaling may regulate weight gain through effects on appetite.

Glucose homeostasis and insulin sensitivity are maintained by Il-21r$^{-/-}$ *mice fed a HFD*

After 12 weeks on the HFD, mice underwent an oral glucose tolerance test. The glucose excursion rates for both cohorts fed chow were similar (Fig. 1*E*, open blue boxes *vs.* open purple boxes). In comparison, *IL-21R*$^{+/+}$ mice fed a high-fat diet exhibited a 50% reduction in glucose excursion as opposed to the response observed in *il-21r*$^{-/-}$ mice (Fig. 1*E*, open blue circles *versus* open purple circles), reflected by a higher AUC value (Fig. 1*F*, 2.1 X 10^4 + 2.3 X 10^3 *vs.* 1.1 X 10^4 ± 1.1 X 10^3). Thus, *il-21r*$^{-/-}$ mice administered the HFD diet demonstrated improved glucose tolerance compared to *IL-21R*$^{+/+}$ mice (Fig. 1, *E* and *F*).

An insulin tolerance test was performed following 14 weeks on the HFD. Both chow-fed groups exhibited comparable glucose uptake rates (Fig. 1*G*) and AUC values (Fig. 1*H*). *IL-21 R*$^{+/+}$ mice maintained on the HFD demonstrated evidence of insulin resistance, as indicated by reduced glucose uptake rates (Fig. 1*G*, open blue circles *versus* open purple circles) and a 1.7-fold increase in AUC compared to mice receiving the chow diet (Fig. 1*H*). These findings indicate that

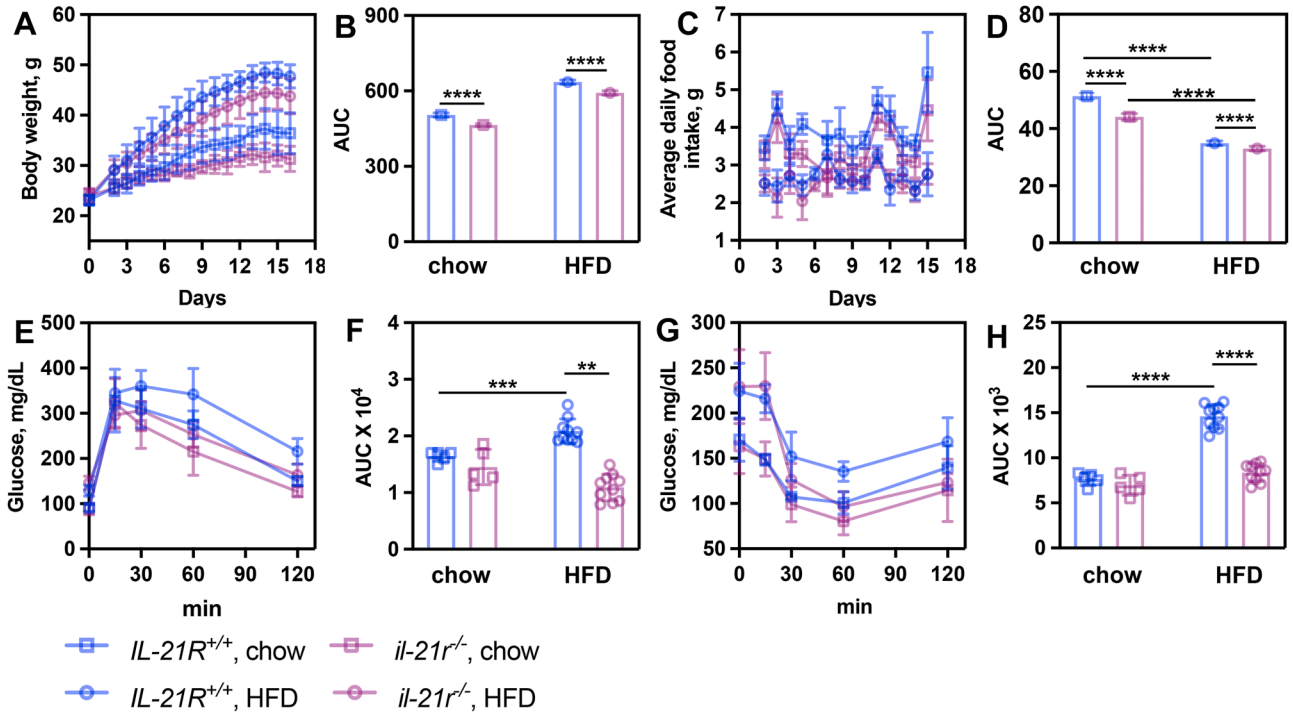

Figure 1. *il21r*$^{-/-}$ mice gain weight on a HFD but maintain glucose tolerance and insulin sensitivity. IL21R$^{+/+}$ (n = 6) and *il21r*$^{-/-}$ (n = 10) mice were fed chow or HFD for 16 weeks; body weight and food intake were recorded weekly. *A*, body weight. *B*, area under the curve. *C*, food intake. *D*, area under the curve, *IL21R*$^{+/+}$ and *il21r*$^{-/-}$ mice were fasted for 16 h, then given 2 g/kg glucose (100 mg/ml) by oral gavage. Blood glucose was measured at 0, 15, 30, 60, and 120 min. *E*, glucose levels over time. *F*, area under the curve (AUC) calculated using data from (*E*). *G*, insulin tolerance test, (*H*), area under the curve (AUC) calculated using data from (*G*). Data were analyzed using two-way ANOVA with Tukey's *post hoc* analysis. Results are reported as mean ± S.D. $^{**}p < 0.001$; $^{***}p < 0.0001$; $^{****}p < 0.00001$. HFD, high-fat diet.

IL-21R signaling plays a significant role in promoting glucose intolerance and insulin resistance.

Il-21r$^{-/-}$ *mice are resistant to HFD-induced MASLD and MASH*

Obesity is a significant risk factor for MASLD/MASH (2, 42). Accordingly, we investigated the potential impact of IL-21R signaling deficiency on HFD-induced MASLD. Liver tissue sections underwent histological staining, and steatosis and fibrosis staging by a veterinary pathologist.

H&E staining showed significant fat accumulation and both micro- and macrovesicular steatosis in the liver of HFD-fed *IL-21R*$^{+/+}$ mice (Fig. 2*A*). Most *IL-21R*$^{+/+}$ mice reached steatosis stage 3 (90%) (Fig. 2*B*, open blue boxes vs. circles), whereas only 3 *il-21r*$^{-/-}$ HFD-fed mice reached stage 1 (Fig. 2*B*, open purple boxes vs. circles).

Trichrome C staining (Fig. 2*C*) revealed no visible signs of fibrosis in either chow-fed cohort. All *IL-21R+/+* mice on the HFD displayed signs of fibrosis, with 40% having a fibrosis stage of 1 and 60% at stage 2 (Fig. 2, *C* and *D*). In contrast, most *il-21r*$^{-/-}$ mice showed no evidence of fibrosis—only 3 out of 10 were assessed at stage 1—suggesting that the majority did not develop MASH (Fig. 2, *C* and *D*).

Il-21r$^{-/-}$ *mice exhibit protection against MASLD due to reduced lipid levels*

The buildup of triglycerides and cholesterol in the liver is linked to MASLD (43). *Il-21r*$^{-/-}$ mice on an HFD showed fewer signs of MASLD. To find out if this was due to differences in lipid levels, triglyceride and cholesterol concentrations were measured in both the blood and liver of these mice.

Chow-fed *il-21r*$^{-/-}$ mice showed reductions of 39% in blood triglycerides and 46% in cholesterol compared to *IL-21R+/+* mice (Fig. 3, *A* and *B*, open blue boxes vs. open purple boxes). In HFD-fed mice, triglyceride concentrations were significantly lower than those in chow-fed groups (Fig. 3, *A* and *B*, open blue circles and open purple circles*)*. Specifically, triglyceride levels decreased by 28% in *IL-21R*$^{+/+}$ mice and by 32% in *il-21r*$^{-/-}$ mice (Fig. 3*A*). Although cholesterol levels increased 2.9-fold and 5.6-fold in HFD-fed *IL-21R*$^{+/+}$ and *il-21r*$^{-/-}$ mice, respectively, both chow and HFD-fed *il-21r*$^{-/-}$ mice had lower cholesterol than their *IL-21R*$^{+/+}$ counterparts (Fig. 3*B*).

In chow-fed *il-21r*$^{-/-}$ mice, hepatic triglyceride levels were reduced by 29% relative to those observed in *IL-21R*$^{+/+}$ counterparts (Fig. 3*C*; open blue boxes vs. open purple boxes). Following HFD administration, triglyceride concentrations increased by 4.1-fold and 6.1-fold in *IL-21R*$^{+/+}$ and *il-21r*$^{-/-}$ mice, respectively, compared to their chow-fed controls; however, *il-21r*$^{-/-}$ mice continued to exhibit a 30% decrease in triglyceride levels compared to HFD-fed *IL-21R*$^{+/+}$ mice (Fig. 3*C*; open blue circles vs. open purple circles). Regarding hepatic cholesterol, HFD feeding resulted in a 20% reduction in *IL-21R*$^{+/+}$ mice and a 32% reduction in *il-21r*$^{-/-}$ mice (Fig. 4*D*).

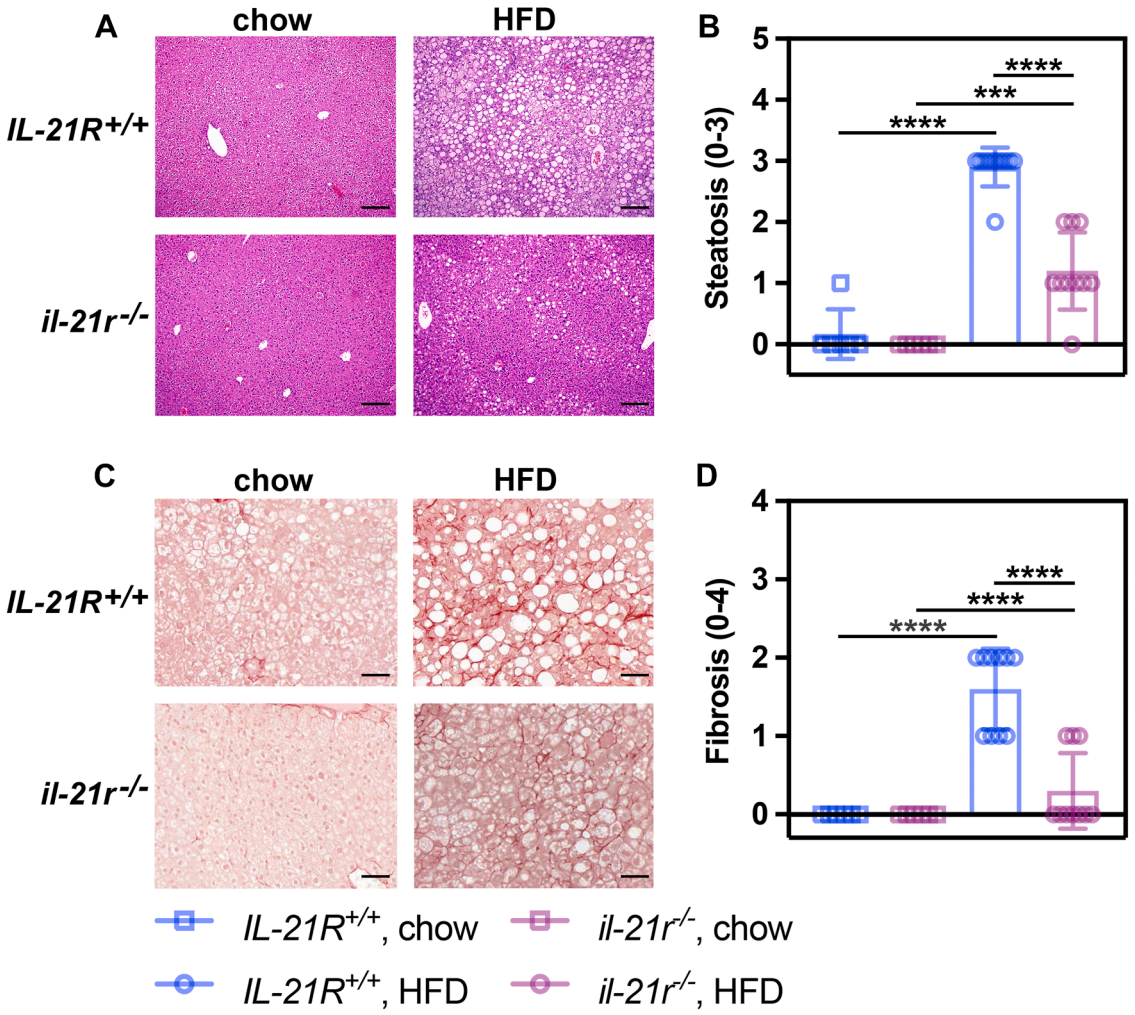

Figure 2. *il21r*$^{-/-}$ mice on a HFD show reduced signs of metabolic dysfunction-associated steatotic liver disease and metabolic dysfunction-associated steatohepatitis. Liver from *IL21 R*$^{+/+}$ (n = 6) and *il21r*$^{-/-}$ (n = 10) mice were analyzed for the levels of steatosis and fibrosis using H&E and trichrome C staining, respectively. *A*, H&E staining of liver tissue sections of chow or HFD-fed mice. *B*, average steatosis stage values. *C*, trichrome C staining of liver tissue sections of chow or HFD-fed mice. *D*, average fibrosis stage values. Data were analyzed using two-way ANOVA with Tukey's *post hoc* analysis. Results are reported as mean ± S.D. ***$p < 0.0001$; ****$p < 0.00001$. A, bar = 40 μm. *B*, bar = 200 μm. HFD, high-fat diet.

Il-21r$^{-/-}$ *mice show resistance to advanced liver damage*

MASLD results in hepatocyte lipotoxicity and liver dysfunction and is typically associated with increased liver enzyme levels (44). The levels of alanine aminotransferase (ALT), aspartate aminotransferase (AST), and alkaline phosphatase were determined. Creatine kinase levels were additionally measured as an indicator of hepatic dysfunction (45).

Both cohorts fed an HFD exhibited increases in ALT and AST compared to mice on a standard chow diet (Fig. S2, *A* and *B*), though *il-21r*$^{-/-}$ mice showed smaller fold changes than *IL-21R*$^{+/+}$ mice. Specifically, ALT rose 6-fold in *IL-21R*$^{+/+}$ mice, while *il-21r*$^{-/-}$ mice experienced only a 2.6-fold increase relative to chow-fed controls. For AST, *IL-21R*$^{+/+}$ mice displayed a 2.6-fold increase *versus* a 1.5-fold rise in *il-21r*$^{-/-}$ mice, when compared to values from chow-fed animals. alkaline phosphatase levels increased 1.5-fold only in *IL-21R*$^{+/+}$ mice on the HFD (Fig. S2*C*). Additionally, creatine kinase—a marker elevated in liver injury (46)—was raised 2.4-fold in *IL-21R*$^{+/+}$ HFD mice (Fig. S2*D*), whereas *il-21r*$^{-/-}$ mice maintained stable levels regardless of diet. Therefore, inhibition of *IL-21R* signaling provides protection against hepatic injury, thereby reducing the severity of HFD-induced MASLD and MASH.

IL-21R levels are elevated in mice with MASH

IL-21R expression is elevated in the liver of patients diagnosed with MASH-driven hepatocellular carcinoma (17, 47). If the reduction observed in MASLD/MASH is due to loss of IL-21R signaling, it follows that IL-21R gene and/or protein expression levels may be higher in *IL-21R*$^{+/+}$ mice fed a HFD.

Liver of *IL-21R*$^{+/+}$ mice on a HFD showed a sixfold increase in *IL-21R* mRNA expression compared to chow-fed mice (Fig. 4*A*). IHC staining showed higher levels in HFD-fed mice than those on chow (Fig. 4*B*). Western analysis revealed markedly higher IL-21R levels in *IL-21R*$^{+/+}$ mice on a HFD than those on chow (Fig. 4*C*). Protein levels were increased by 50-fold in HFD-fed *IL-21R*$^{+/+}$ mice (Fig. 4*D*). Thus, elevated levels of IL-21R are closely associated with the onset and progression of MASH.

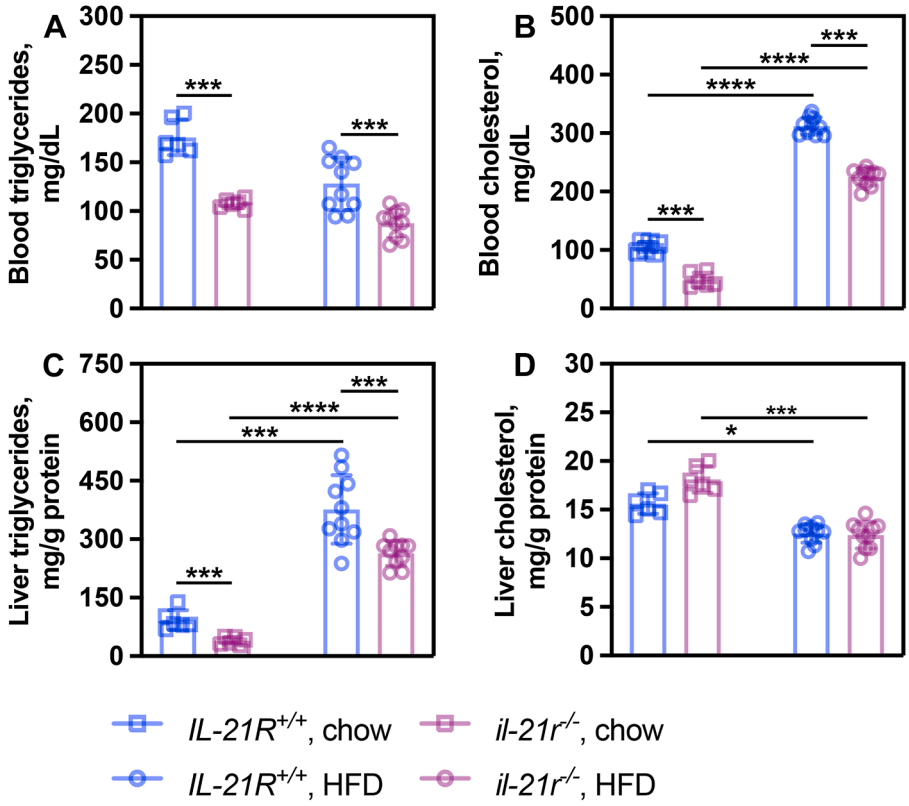

Figure 3. *il21r–/–* mice demonstrate reduced triacylglycerides levels and exhibit indications of liver improvement when fed a HFD. Blood and liver from *IL21 R*$^{+/+}$ (n = 6) and *il21r*$^{-/-}$ (n = 10) mice fed chow or a HFD were analyzed for lipids and liver enzyme levels. *A*, blood triglycerides levels. *B*, blood cholesterol levels. *C*, liver triglycerides levels. *D*, liver cholesterol levels. Data were analyzed using two-way ANOVA with Tukey's *post hoc* analysis. Results are reported as mean ± S.D. **$p < 0.001$; ***$p < 0.0001$; ****$p < 0.00001$. HFD, high-fat diet.

IL-21R is overexpressed in the liver of individuals with fatty liver and nodular cirrhosis

Liver from people with MASH-driven hepatocarcinoma have high *IL-21R* expression (17). It is unclear if IL-21 accumulation and increased signaling appears prior to HCC development or later and drives its progression.

Liver tissue sections from normal (n = 11), fatty liver (n = 14), and nodular cirrhosis (n = 31) patients were stained to assess IL-21R levels (Fig. 4*E*). IL-21R levels rose as fatty liver developed and showed further increase in liver tissues from individuals that had transitioned from MASH to nodular cirrhosis (Fig. 5*F*).

Il-21r$^{-/-}$ *mice fed a HFD have reduced collagen deposition in their liver*

il-21r$^{-/-}$ fed a HFD showed reduced numbers of fibrotic-like structures by histology and a reduced average fibrotic stage. Hepatic stellate cell (HSC) activation is a critical step in progressing MASLD to MASH (48). HSCs activate early in MASH, adopting a myo-fibroblast phenotype and are responsible for liver collagen deposition during disease progression (49). To assess whether HSCs were activated in HFD-fed *IL-21R*$^{+/+}$ mice, we measured the protein levels of collagen 1α 1 chain (COL1A1), a smooth muscle actin (αSMA) (a myofibroblast marker), and vimentin, which has been shown to be elevated in activated HSCs (50).

Protein levels of COL1A1, αSMA, and Vimentin increased in *IL-21R*$^{+/+}$ mice on a HFD but were markedly reduced in *il-21r*$^{-/-}$ mice (Fig. 5*A*). In *il-21r–/–* mice, COL1A1 decreased 4.3-fold, αSMA 23-fold, and vimentin 4.2-fold compared to *IL-21R*$^{+/+}$ mice (Fig. 5, *B–D*).

TGFβ-1 is secreted during the early stages of liver injury and serves as a key activator of HSCs in the progression from MASLD to MASH (51, 52). It is produced as an inactive complex that can be activated by reactive oxygen species, thrombospondin-1, and specific proteases (52). To further assess HSC activation, both total and active TGFβ-1 concentrations were measured in blood and liver samples.

Total TGFβ-1 blood concentrations exhibited a 1.7-fold increase in *IL-21R*$^{+/+}$ mice subjected to an HFD compared to those fed chow, while levels remained at baseline in *il-21r*$^{-/-}$ mice (Fig. 5*E*). Active TGFβ-1 blood concentrations were substantially elevated in *IL-21R*$^{+/+}$ mice on the HFD (11-fold) relative to chow-fed controls but showed a more modest rise (7-fold) in *il-21r*$^{-/-}$ mice, remaining 62% lower than those observed in *IL-21R*$^{+/+}$ mice (Fig. 5*G*).

Total liver TGFβ-1 levels were stable regardless of group or diet (Fig. 5*F*). However, HFD-fed *IL-21R*$^{+/+}$ mice showed a 4.1-fold rise in active TGFβ-1, which did not occur in *il-21r*$^{-/-}$

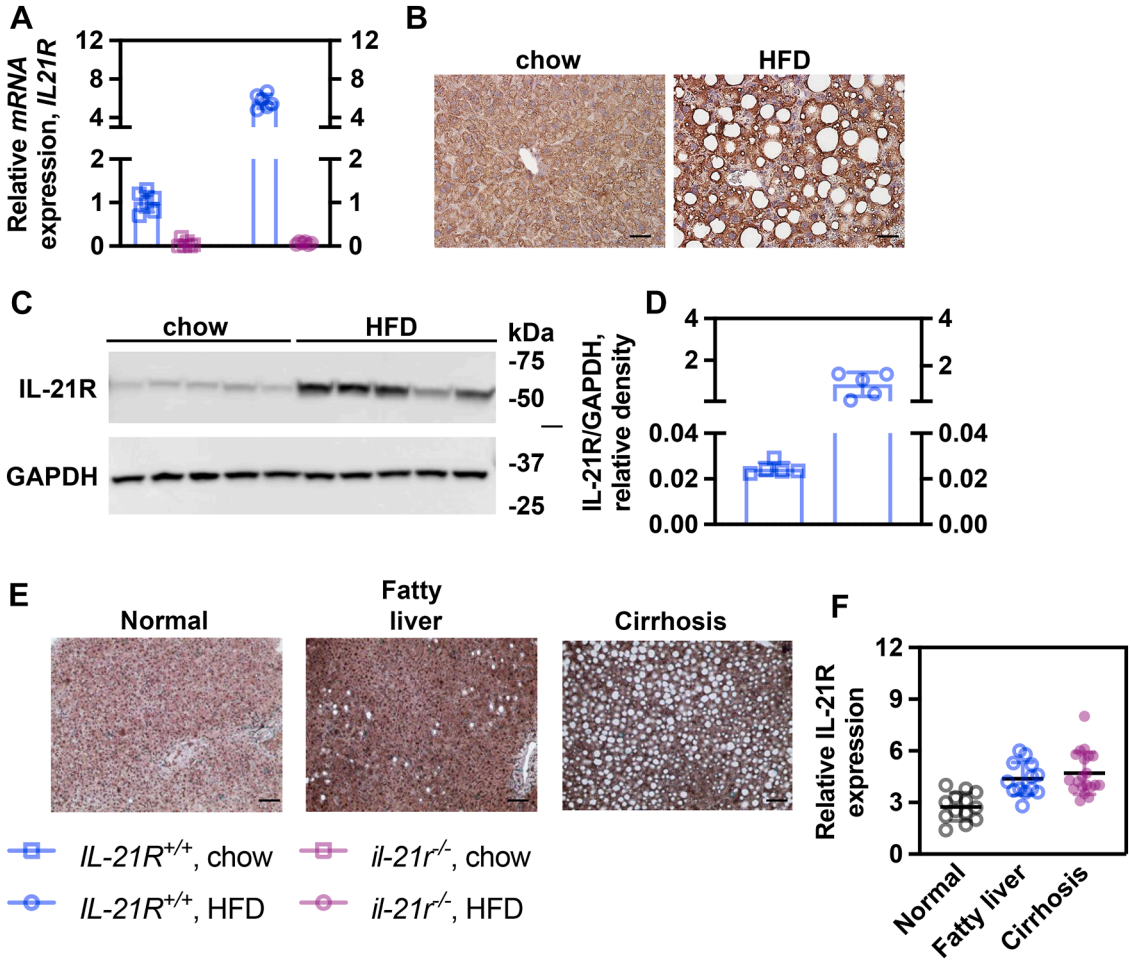

Figure 4. *IL-21 R* gene expression and protein levels are elevated in *IL-21R*$^{+/+}$ mice on a HFD. Total RNA was extracted from the liver of *IL21 R*$^{+/+}$ mice fed chow (n = 6) or a HFD (n = 6) and *IL-21R* gene expression levels were determined using *q*RT-PCR. *A*, *IL-21R* gene expression levels. Liver tissue sections from *IL21 R*$^{+/+}$ mice fed chow or a HFD were used to determine the protein levels of IL-21R by immunohistochemical staining using anti-IL-21R antibodies. *B*, protein levels of IL-21R determined by IHC. Panels are representative of three individual liver. Liver from *IL21 R*$^{+/+}$ and *il21r*$^{-/-}$ mice fed chow or a HFD were used to determine the protein levels of IL-21R by western analysis (n = 5). *C*, western analysis of IL-21R. *D*, relative densitometry levels of IL-21R. GAPDH was used as a loading control. Image J software was used to determine densitometry levels. *E*, a tissue microarray (USBioMax LV1201 B) was immunostained against IL-21R using human IL-21R antibodies and exposed using 3,3′-diaminobenzidine (DAB) and counterstained with hematoxylin. Protein expression was quantified using Image J software as described (89). *F*, fatty liver quantification compared to normal tissue was significant with a 1.3-fold increase ($p < 0.001$). Cirrhosis quantification compared to normal tissue was significant with a 1.4-fold increase ($p < 0.01$). An unpaired two-tailed *t* test was used for statistical analysis. Data were analyzed using two-way ANOVA with Tukey's *post hoc* analysis. Results are reported as mean ± S.D. *$p < 0.01$; ****$p < 0.00001$. B, bar = 60 μm. *D*, 40 μm. IL-21R, interleukin-21 receptor; HFD, high-fat diet.

mice; active TGFβ-1 levels remained unchanged in HFD-fed *il-21r*$^{-/-}$ mice compared to those on chow (Fig. 5*H*).

Therefore, high amounts of active liver TGF-β1 in *IL-21R*$^{+/+}$ mice promote hepatic stellate cell (HSC) activation and increase collagen buildup, resulting in fibrosis. In contrast, *il-21r*$^{-/-}$ mice fed an HFD do not show increased TGF-β1 levels, which is associated with reduced collagen deposition and less liver fibrosis.

IL-21R-dependent JAK-STAT signaling is dampened in Il-21r$^{-/-}$ *mice*

IL-21 binding to the IL-21R triggers JAK-STAT signaling that drives differentiation of multiple T cell populations that include Th17, Tfh, Tcm, and B cells, and promotes macrophage transition from the M2 to M1 pro-inflammatory phenotype (11). To evaluate IL-21R signaling in mice fed a HFD, a JAK-STAT protein microarray was used to measure phosphorylation levels-activation status of various JAK-STAT proteins in liver.

JAK1 expression increased in both groups fed an HFD, but the rise was less pronounced in *il-21r*$^{-/-}$ mice (2.2-fold *vs.* 1.4-fold) (Fig. S3). Additionally, only *IL-21R*$^{+/+}$ mice showed upregulated JAK2 levels when fed a HFD (6.7-fold); by contrast, *il-21r*$^{-/-}$ mice maintained JAK2 expression similar to that of chow-fed controls (Fig. S3). Interestingly, while pSTAT1^{Ser727} levels were comparable among chow-fed *IL-21R*$^{+/+}$ and *il-21r*$^{-/-}$ mice as well as HFD-fed *IL-21R*$^{+/+}$ mice, these levels were reduced in HFD-fed *il-21r*$^{-/-}$ mice, suggesting that IL-21R signaling is necessary to maintain basal pSTAT1 activity under HFD conditions. Both pSTAT2^{Tyr689} and pSTAT3Tyr^{705} were elevated in HFD-fed *IL-21R*$^{+/+}$ mice, whereas these levels dropped below baseline in *il-21r*$^{-/-}$ mice (Fig. S3) compared to chow-fed mice. Finally, pSTAT5^{Tyr694}

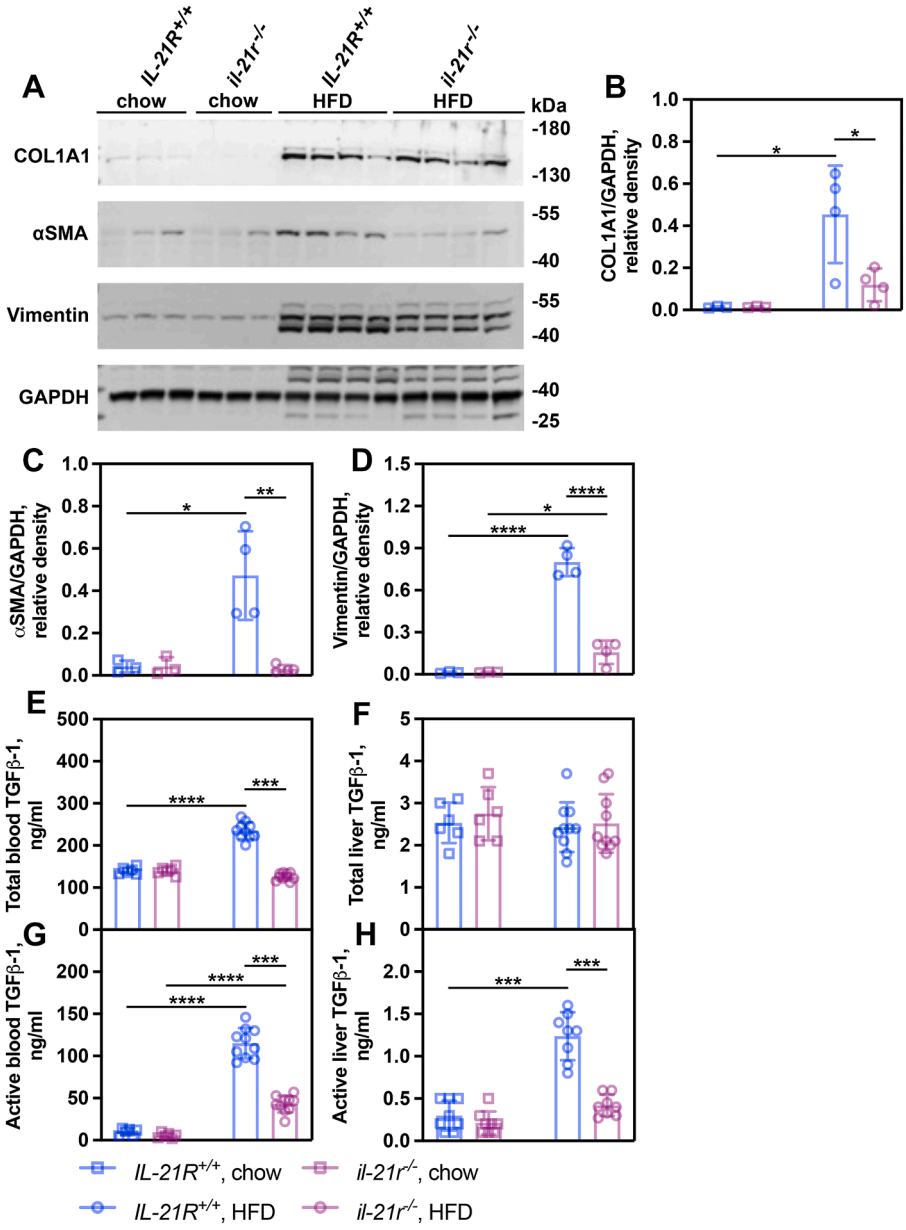

Figure 5. Hepatic stellate cell activation is dampened in *il21r–/–* mice. Liver from *IL21 R*$^{+/+}$ (n = 3, chow; n = 4, HFD) and *il21r*$^{-/-}$ (n = 3, chow; n = 4, HFD) mice fed chow or a HFD were analyzed for protein. *A*, collagen 1α 1 chain, a smooth muscle actin, and vimentin protein levels by western analysis. *B*, relative densitometry levels of collagen 1α 1 chain. *C*, relative densitometry levels of a smooth muscle actin. *D*, relative densitometry levels of vimentin. GAPDH was used as a loading control. Image J software (imagej.net/software) was used to determine densitometry levels. Total and active TGFβ-1 blood and liver levels were measured as described in "Experimental procedures". *E*, total blood TGFβ-1 levels. *F*, active TGFβ-1 blood levels. *G*, total liver TGFβ-1 levels. *H*, active liver TGFβ-1 levels. Data were analyzed using two-way ANOVA with Tukey's *post hoc* analysis. Results are reported as mean ± S.D. *$p < 0.01$; **$p < 0.001$; ***$p < 0.0001$; ****$p < 0.00001$. HFD, high-fat diet.

levels were markedly elevated in *IL-21R*$^{+/+}$ mice on a high-fat diet (3.8-fold), whereas this elevation was attenuated by 70% in *il-21r*$^{-/-}$ mice receiving the same diet, and by 20% relative to the basal levels observed in *IL21*$^{+/+}$ mice maintained on chow.

To confirm the microarray findings, protein levels were measured using western blotting and ELISA for pJAK1-^{Tyr1022}—a marker of JAK1 activation—as well as pSTAT3-^{Tyr705} and pSTAT5^{Tyr694}, which are phosphorylation sites that change during IL-21R signaling activation (11).

Both *IL-21R*$^{+/+}$ and *il-21r*$^{-/-}$ mice maintained on a chow diet exhibited low basal levels of pJAK1^{Tyr1022} (Fig. 6, *A* and *B*). Significantly higher levels were observed in *IL-21R*$^{+/+}$ mice subjected to a high-fat diet (HFD), with a more modest increase detected in *il-21r*$^{-/-}$ mice under similar dietary conditions (Fig. 6, *A* and *B*). Specifically, pJAK1^{Tyr1022} levels increased by 3.7-fold in *IL-21R*$^{+/+}$ mice receiving the HFD, whereas a 2.2-fold elevation was seen in *il-21r*$^{-/-}$ mice compared to their respective chow-fed controls (Fig. 6*B*). Chow-fed *il-21r*$^{-/-}$ mice showed lower pSTAT3^{Tyr705} levels than *IL-21R*$^{+/+}$ mice, with a further decrease under HFD conditions. In contrast, high-fat diet increased these levels 3.3-fold in *IL-21R*$^{+/+}$ mice (Fig. 6*C*). Both chow groups had

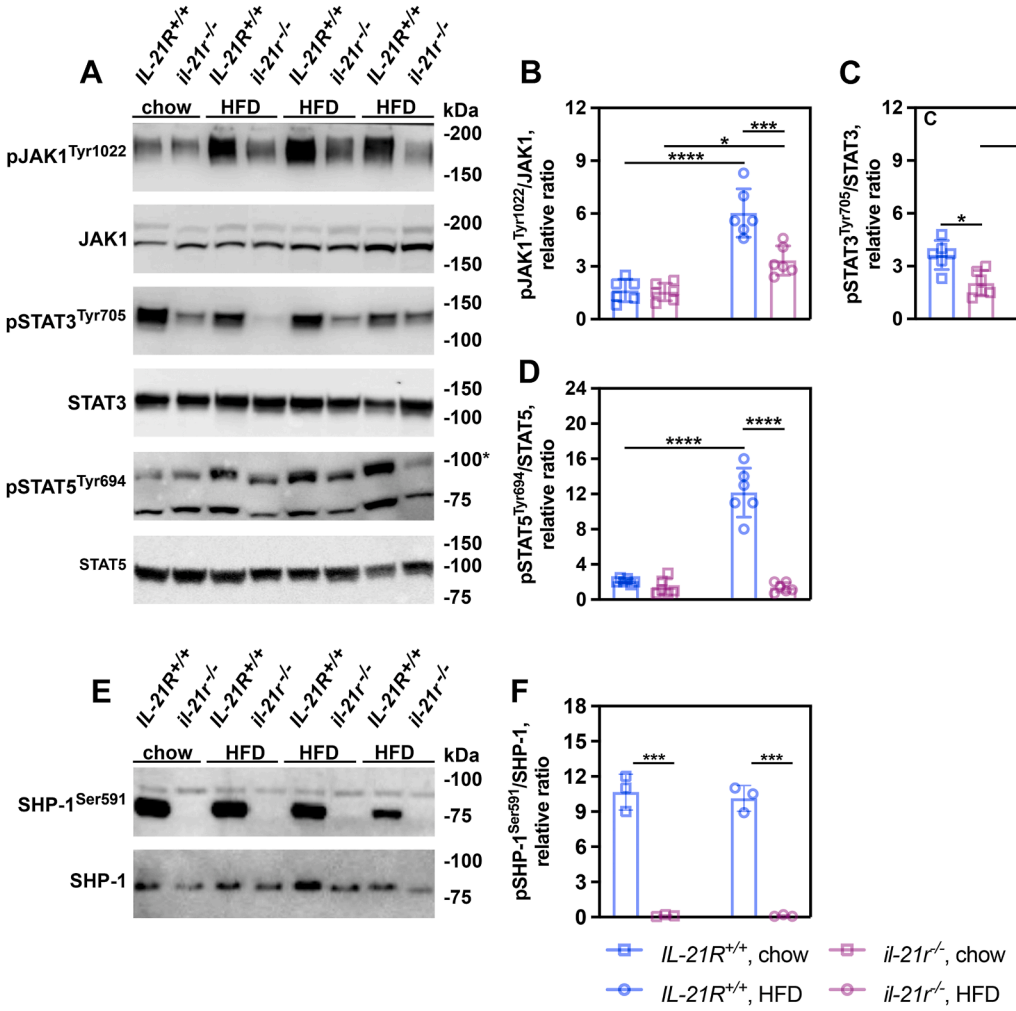

Figure 6. *il21r–/–* mice show reduced pJAK-pSTAT signaling on a HFD. Liver of *IL21 R*$^{+/+}$ and *il-21r*$^{-/-}$ mice fed chow (n = 3) or a HFD (n = 3) were used for western analysis of phosphophorylated and total JAK1, STAT3, and STAT5 levels. *A*, protein levels of pJAK1^{Tyr1022}, JAK1, pSTAT3^{Tyr705}, STAT3, pSTAT5T^{yr694}, and STAT5 were determined by western analysis. Panels indicating the protein levels in chow-fed mice are representative of n = 3 mice. ELISA assays were performed on mice fed chow or a HFD (n = 6). *B*, protein levels of pJAK1^{Tyr1022}. *C*, protein levels of pSTAT3^{Tyr705}. *D*, protein levels of pSTAT5T^{yr694}. The levels of pJAK1^{Tyr1022}, pSTAT3^{Tyr705}, and pSTAT5T^{yr694}, were determined by dividing the values obtained for the phosphorylated form of the protein divided by the levels of the total protein. Livers of *IL21R*$^{+/+}$ and *il-21r*$^{-/-}$ mice fed chow or a HFD were used for western analysis of phosphophorylated pSHP-1^{Ser591} and total SHP-1 (n = 3). *E*, western analysis of pSHP-1^{Ser591} and SHP-1 by western analysis. Panels indicating the protein levels in mice are representative of n = 3 mice. *F*, Relative densitometry values for pSHP-1^{Ser591} levels. Image J software was used to determine densitometry levels. The levels of pJAK1^{Tyr1022}, pSTAT3^{Tyr705}, pSTAT5T^{yr694}, and pSHP-1^{Ser591}were determined by dividing the values obtained for the phosphorylated form of the protein divided by the levels of the total protein. Data were analyzed using two-way ANOVA with Tukey's *post hoc* analysis. Results are reported as mean ± S.D. *$p < 0.01$; ***$p < 0.0001$; ****$p < 0.00001$. IL-21R, interleukin-21 receptor; HFD, high-fat diet.

similar pSTAT5^{Tyr694} levels; however, HFD led to a 6-fold rise in *IL-21R*$^{+/+}$ mice, which was absent in HFD-fed *il-21r*$^{-/-}$ mice (Fig. 6*D*).

The SHP-1 phosphatase dephosphorylates multiple factors in the JAK-STAT pathway (53). Its activity is inhibited by phosphorylation at Ser591 (54). Microarray analysis showed higher SHP-1^{Ser591} levels in *IL-21R*$^{+/+}$ mice fed the HFD than in *il-21r*$^{-/-}$ mice (data not shown). Western analysis was used to determine the levels of pSHP-1^{Ser591}.

SHP1^{Ser591} levels rose over 100-fold in *IL-21R*$^{+/+}$ mice on either diet but were nearly undetectable in *il-21r*$^{-/-}$ mice (Fig. 6, *E* and *F*). This indicates that SHP-1 activity is inhibited by feeding the HFD to *IL-21R*$^{+/+}$ mice but stays active in *il-21r*$^{-/-}$ mice. JAK1-STAT5 signaling also decreased in *il-21r*$^{-/-}$ mice on a high-fat diet, likely due to enhanced SHP-1 phosphatase activity.

HIF-2α-dependent transcription of de novo *lipogenesis is reduced in* il-21r$^{-/-}$ *mice*

HIF-2α activity increases during MASH, promoting *de novo* lipogenic gene expression (55, 56). pSTAT5 enhances HIF-2α by upregulating its expression (57). *il-21r*$^{-/-}$ mice exhibited reduced pSTAT5^{Tyr694} levels and hepatic steatosis. HIF-2α protein levels were assessed by Western blot and ELISA, and its gene targets were evaluated based on lipogenic gene expression.

HIF-2α protein levels were found to be more than three times higher in *IL-21R*$^{+/+}$ mice fed a high-fat diet (HFD) compared to *il-21r*$^{-/-}$ mice (Fig. 7, *A*–*C*). Enhanced expression was also observed for HIF-2α-induced genes involved in fatty acid synthesis, specifically *SREBF1* and *FASN*, as well as the fatty acid transporter gene *CD36* and the lipid droplet-associated gene *PLIN2*. In *il-21r*$^{-/-}$ mice, expression of

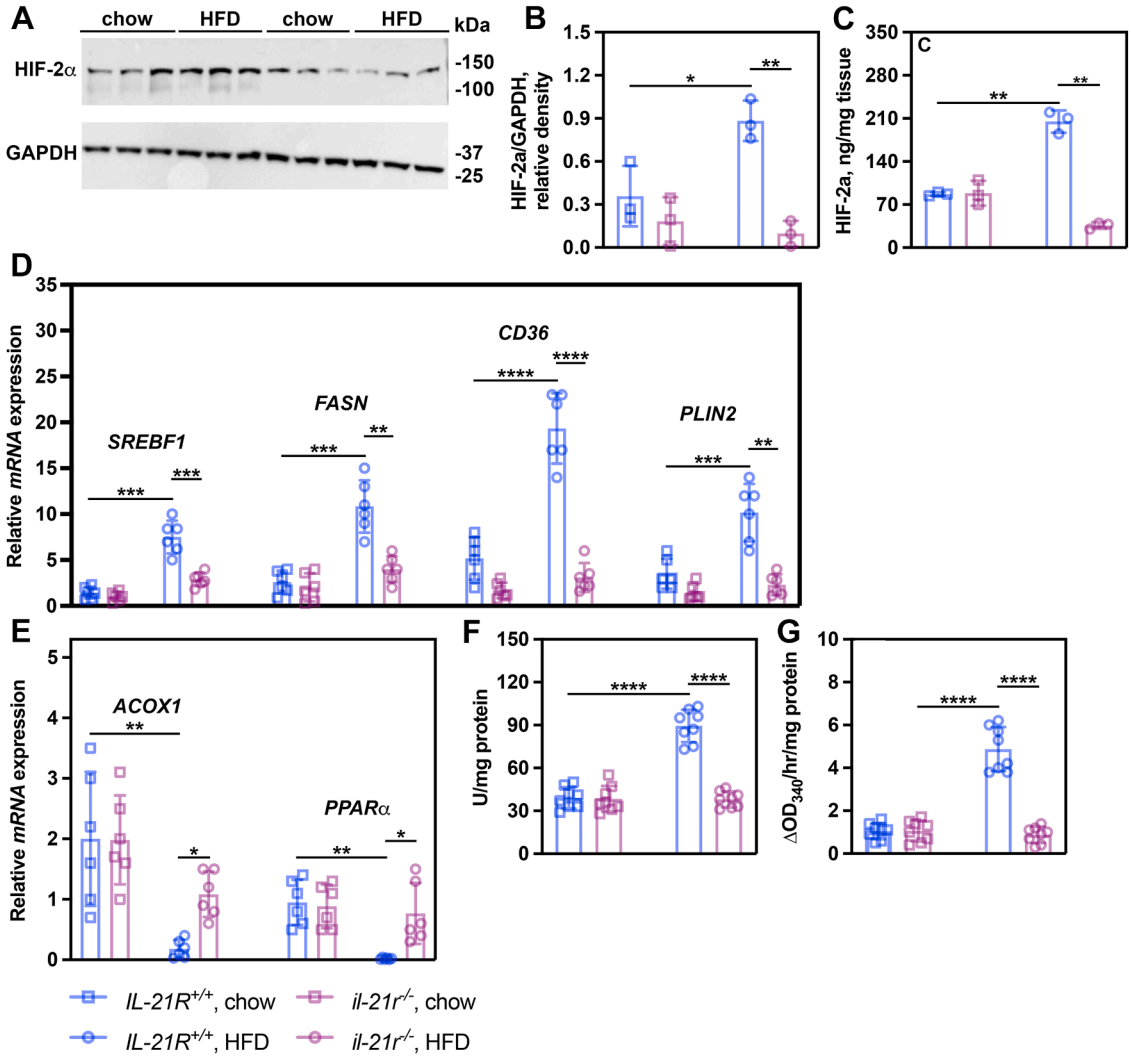

Figure 7. HIF-2α-mediated lipogenic gene expression is diminished in il-21r mice on a HFD. Livers of *IL21R*$^{+/+}$ and *il-21r*$^{-/-}$ mice fed chow or a HFD were used for western analysis to determine protein levels (n = 3). *A*, HIF-2a protein levels by western analysis. *B*, densitometry levels of HIF-2a. Densitometry values were determined using Image J software. GAPDH was used as a loading control. Protein levels were assessed by ELISA in liver samples obtained from both cohorts (n = 6). *C*, HIF-2a protein levels using ELISA. Livers of *IL21R*$^{+/+}$ and *il-21r*$^{-/-}$ mice fed chow or a HFD were used for *q*RT-PCR analysis to determine gene expression levels (n = 6). *D*, HIF-2a-dependent upregulated gene expression levels. *E*, HIF-2a-dependent down regulated gene expression levels. *F*, ACC1 enzyme assay. *G*, FASN enzyme assay. Data were analyzed using two-way ANOVA with Tukey's post hoc analysis. Results are reported as mean + S.D. *$p < 0.01$; **$p < 0.001$; ***$p < 0.0001$; ****$p < 0.00001$. IL-21R, interleukin-21 receptor; HFD, high-fat diet.

these genes was reduced to basal levels (58, 59)} (Fig. 7*D*). Conversely, elevated expression levels of the HIF-2α-repressed target genes acyl-CoA oxidase 1 and peroxisome proliferator-activated receptor α were detected in *il-21r*$^{-/-}$ mice on an HFD (Fig. 8*E*).

To further assess whether the loss of IL-21R signaling affects *de novo* lipogenesis, we measured the enzyme activities of acetyl-CoA carboxylase 1 (ACC1) and fatty acid synthase (FASN) (Fig. 7, *F* and *G*).

Comparable levels of ACC1 and FASN activity were observed in both cohorts fed chow diets (Fig. 7, *F* and *G*). In *IL-21R*$^{+/+}$ mice, ACC1 activity increased by several-fold and FASN activity also rose substantially, whereas these activities remained at baseline chow levels in *il-21r*$^{-/-}$ mice. These findings indicate that *IL-21R*$^{+/+}$ mice fed a high-fat diet exhibited elevated enzymatic activities associated with *de novo* fatty acid synthesis.

The data further suggest that hepatic lipid accumulation in *IL-21R*$^{+/+}$ mice is at least partially attributable to JAK1-STAT5-mediated HIF-2α target gene expression, leading to increased *de novo* lipogenesis. Additionally, the reduced signs of MASLD observed in *il-21r*$^{-/-}$ mice appear to result from the suppression of this JAK1-STAT5 induced, HIF-2α-dependent expression, which contributes to diminished lipid synthesis.

HIF-2α-dependent mammalian target of rapamycin complex 1 activation and inhibition of autophagy is repressed in il-21r$^{-/-}$ *mice*

mTORC1 acts as an energy sensor, controlling anabolic signaling based on nutrient levels (60, 61). Its activity decreases during starvation and increases when nutrients are abundant (60). HIF-2α indirectly activates mTORC1 by inducing the levels of the solute carrier family 7 member 5

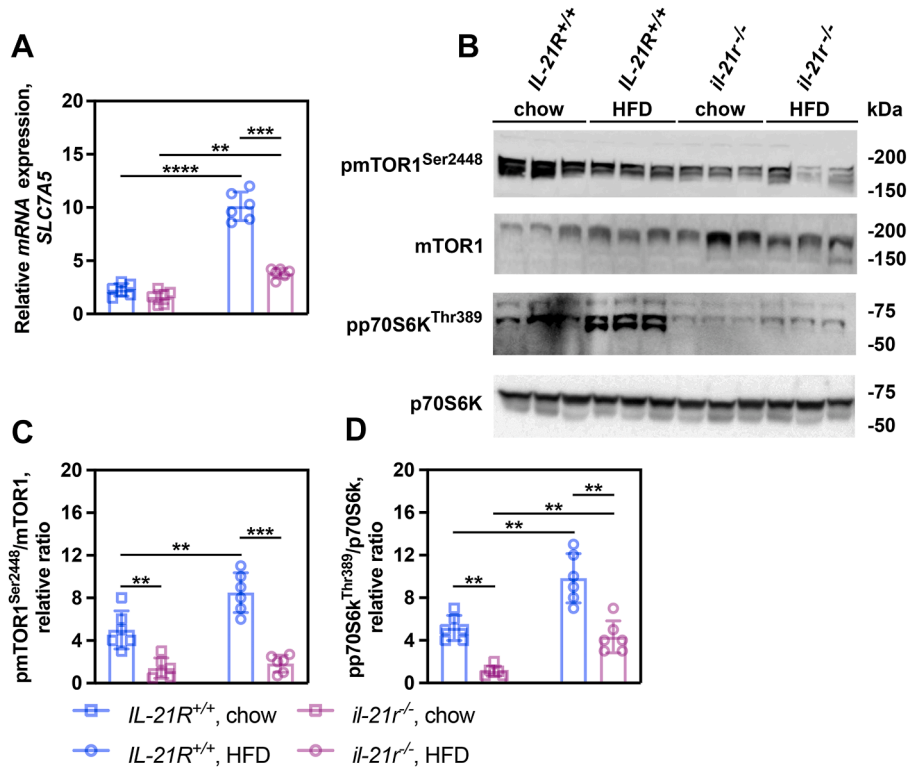

Figure 8. *il-21r*$^{-/-}$ mice show weakened mammalian target of rapamycin complex 1 activity on a HFD. Livers of *IL21 R*$^{+/+}$ and *il-21r*$^{-/-}$ mice fed chow or a HFD were used for *q*RT-PCR analysis to determine gene expression levels (n = 6). *A*, solute carrier family 7 member 5 gene expression levels. Liver of *IL21R*$^{+/+}$ and *il-21r*$^{-/-}$ mice fed chow or a HFD were used for western analysis to determine protein levels (n = 3). *B*, pmTOR1^{Ser2448}, mTOR1, pp70S6K^{Thr389}, and p70S6K protein levels by western analysis. Protein concentrations were assessed by ELISA using liver samples from both cohorts (n = 6). *C*, pmTOR1^{Ser2448} protein levels. *D*, pp70S6K^{Thr389} protein levels. The levels of pmTOR1^{Ser2448} and pp70S6K^{Thr389} were determined by dividing the values obtained for the phosphorylated form of the protein divided by the levels of the total protein. Data were analyzed using two-way ANOVA with Tukey's *post hoc* analysis. Results are reported as mean ± S.D. **$p < 0.001$; ***$p < 0.0001$; ****$p < 0.00001$. IL-21R, interleukin-21 receptor; HFD, high-fat diet.

(SLC7A5) amino acid transporter, leading to amino acid influx and enhanced mTORC1-driven anabolism (62). In this state, mTORC1 suppresses autophagy to maintain macromolecular synthesis (63).

SLC7A5 gene expression levels were measured. mTORC1 signaling was assessed by determining the status of pmTOR1^{Ser2448} phosphorylation by western analysis and ELISA. The phosphorylated levels of the mTORC1 target, pp70S6K^{Thr389}, were also determined to ascertain the level of mTORC1 activity.

Gene expression analysis revealed that *SLC7A5* levels were elevated by 4.5-fold in *IL-21R*$^{+/+}$ mice receiving an HFD, compared to a 2.1-fold increase observed in *il-21r*$^{-/-}$ mice (Fig. 8*A*). Furthermore, *il-21r*$^{-/-}$ mice fed an HFD exhibited a 60% reduction in gene expression relative to chow-fed controls. Protein analysis demonstrated that pmTOR1^{Ser2448} levels increased in *IL-21R*$^{+/+}$ mice on the HFD, while remaining at baseline chow-fed levels in the *il-21r*$^{-/-}$ group (Fig. 8, *B* and *C*). Additionally, HFD-fed *IL-21R*$^{+/+}$ mice showed heightened mTOR activity-dependent pp70S6K^{Thr389} levels, whereas *il-21r*$^{-/-}$ mice displayed a marked decrease (Fig. 8, *B* and *D*).

mTORC1 is known to inhibit autophagy. Phosphorylated p62/sequestosome-1 (pp62^{Ser403}) functions as a nucleating factor in the degradation of ubiquitinated proteins (64). Its accumulation is associated with MASH, facilitating Mallory-Denk body formation and inducing hepatocyte cell death (65). Additionally, pp62$^{Thr269/Ser272}$ has been shown to accumulate under conditions of impaired autophagy and increased aggresome formation (66). We reasoned that if mTORC1 was active, autophagy should be inhibited. We measured the levels of pp62 in liver of mice fed the various diets.

Western blot analysis indicated that pp62^{Ser403} and pp62Thr$^{269/Ser272}$ levels were higher in *IL-21R*$^{+/+}$ mice fed an HFD compared to *il-21r*$^{-/-}$ mice on the same regimen (Fig. 9, *A*–*C*). Notably, both genotypes exhibited similar overall p62 protein abundance under HFD conditions (Fig. 9*A*). However, in *il-21r*$^{-/-}$ mice, the p62 protein was not converted into its phosphorylated forms associated with autophagy inhibition.

LC3-I protein is involved in autophagosome formation for the degradation of cellular macromolecules during autophagy (67). During autophagy it is lipidated and converted to its active form LC3-II. A high LC3-II:LC3-I ratio is a marker for ongoing autophagy (68). LC3-I and LC3-II levels were determined using ELISA.

All mice maintained on chow demonstrated normal autophagic flux, as indicated by a high LC3-II to LC3-I ratio (~3.5) (Fig. 9*D*). This ratio decreased to approximately 0.6 in *IL-21R*$^{+/+}$ mice fed a high-fat diet (HFD), whereas autophagy was markedly elevated in *il-21r*$^{-/-}$ mice, with a ratio of approximately 2.2.

Proteins targeted for pp62-dependent degradation are marked by K48-linked ubiquitin as a degradation signal (69).

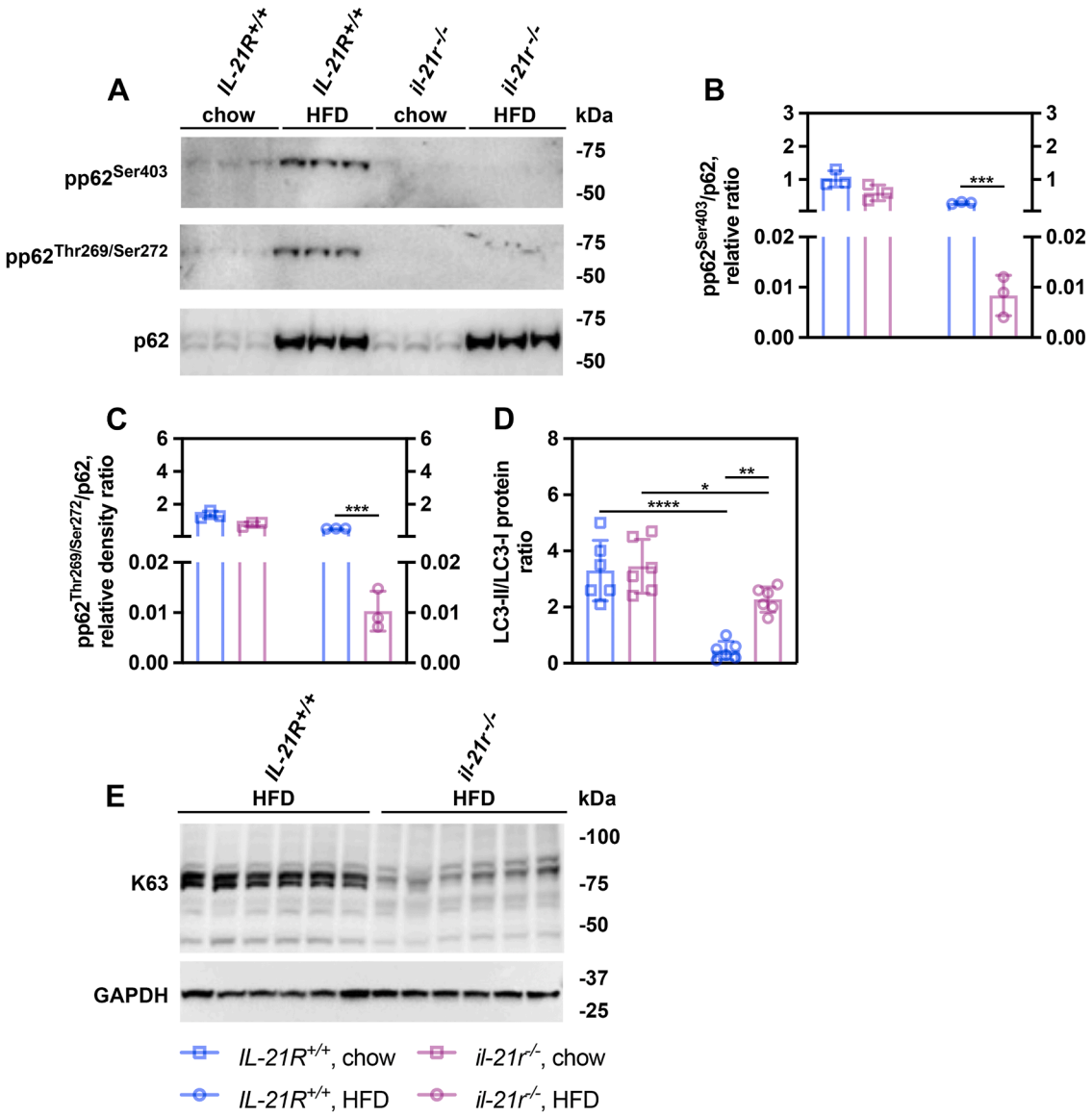

Figure 9. Il-21r–/– mice fed a HFD maintain autophagy on a HFD. Liver of *IL21 R*$^{+/+}$ and *il-21r*$^{-/-}$ mice fed chow or a HFD were used for western analysis to determine protein levels (n = 3). *A*, pp62^{Ser403}, pp62$^{Thr269/Ser272}$, and p62, levels by western analysis. The levels of pp62^{Ser403} and pp62$^{Thr269/Ser272}$ were determined by dividing the densitometry values obtained for the phosphorylated form of the protein divided by the levels of the total protein. Densitometry values were determined using Image J software. *B*, relative protein levels of pp62^{Ser403}. *C*, relative protein levels of pp62$^{Thr269/Ser272}$. Liver of *IL21 R*$^{+/+}$ and *il-21r*$^{-/-}$ mice fed chow or a HFD were analyzed by ELISA to determine protein levels (n = 6). *D*, protein levels of LC3-I and LC3-II. Liver of *IL21 R*$^{+/+}$ and *il-21r*$^{-/-}$ mice fed chow or a HFD were analyzed by western blotting to determine protein levels (n = 5). *E*, protein levels of K48-ubiquitinated proteins. IL-21R, interleukin-21 receptor; HFD, high-fat diet.

The levels of K48-ubiquitinated proteins were determined by western analysis.

Liver from *IL-21R*$^{+/+}$ mice fed a high-fat diet accumulated high levels of K48-ubiquitinated proteins (Fig. 9*E*), while *il-21r*$^{-/-}$ mice on the same diet showed reduced accumulation.

Overall, our *in vivo* results show that activated IL-21R signaling during MASH enhances pJAK1-pSTAT5 signaling, which induces HIF-2α transcription and increased *SLC7A5* expression, leading to mTORC1 activation and autophagy inhibition. IL-21 R deficiency mitigates the progression of MASLD and MASH by inhibiting mTORC1 activity, which consequently restores autophagy in *il-21r*$^{-/-}$ mice subjected to a HFD.

IL-21R co-localizes with CD4+ cells in fatty liver

CD4^{+} T cells produce IL-21 (70). When located in the liver, these T cells can serve as a source of IL-21 and contribute to IL-21R signaling. Immunohistochemistry (IHC) of CD4 was used to identify the localization of CD4+ T cells within different human liver tissue samples, with a focus on their spatial relationship to IL-21R expression.

IL-21R protein expression levels rose during fatty liver and nodular cirrhosis (Fig. 10, IL2R). As disease progression occurred, CD4^{+} T cell levels also increased (CD4) and co-localized with IL-21R (Fig. 10, merged).

The findings strongly suggest that IL-21R signaling is activated in MASH *via* the migration of inflammatory CD4+

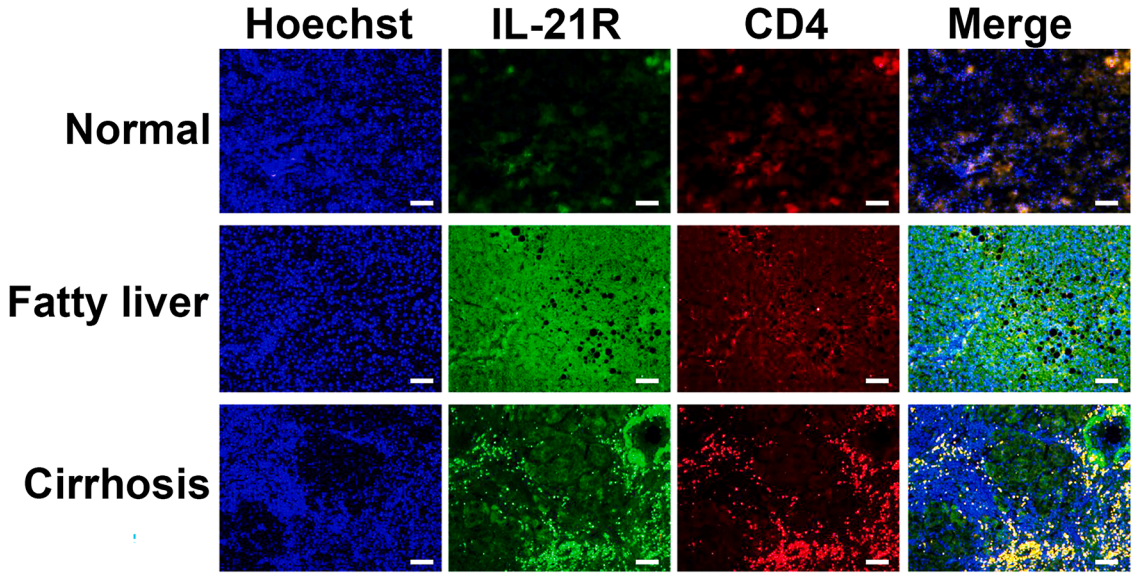

Figure 10. IL-21 R co-localizes with CD4 in human liver tissues sections from patients with fatty liver and nodular cirrhosis. Tissue sections were obtained from NOVUS Biologics and co-stained against IL-21R and CD4 antibodies. Images were taken using a Leica DRME fluorescence microscope. IL-21R, interleukin-21 receptor; HFD, high-fat diet.

T cells to the liver, which provide the IL-21 necessary for receptor activation.

Discussion

Our findings indicate that IL-21R signaling mediates obesity-induced MASLD/MASH. Notably, *Il-21r*$^{-/-}$ mice do not develop MASLD/MASH when subjected to a HFD, presumably because the absence of IL-21R inhibits JAK1-STAT5 activation of HIF-2α-dependent transcription and mTORC1 activity, thereby decreasing lipogenesis and the suppression of autophagy. We also demonstrate that fatty or cirrhotic human liver have increased IL-21R protein, which co-localizes with CD4 on T helper cells—key coordinators of immune response and T cell migration (71).

Murine genetic models indicate that JAK-STAT signaling has multiple roles in MASH regulation. Mice with adipocyte-specific JAK2 deletion exhibited increased adiposity but maintained insulin sensitivity (72). In aged mice with hepatic-specific *jak2*$^{hep\Delta-/-}$ deletion, insulin resistance and MASLD/MASH developed, a condition that was alleviated by additional JAK2 ablation in adipocytes (73). In our studies, JAK2 protein levels remained unchanged across both groups regardless of dietary conditions (data not shown).

So far, the involvement of JAK1 in the pathogenesis of MASLD/MASH remains uninvestigated, as its deletion results in embryonic lethality. However, JAK1 phosphorylates and activates STAT5^{Tyr694} after IL-2 signaling during liver inflammation (74, 75). Elevated *JAK1* expression in fibrotic human liver has been observed, and the Jak1/2 inhibitor Ruxolitinib reduces fibrosis severity (76).

Increased pSTAT3 levels were observed in *IL21R*$^{+/+}$ mice and found to be lower in *il21r*$^{-/-}$ mice. Previous research has indicated that STAT3 inhibition *in vivo* can reduce manifestations of MASLD/MASH in mice deficient in hepatic phosphatase and tensin homolog, which serves as a genetic model for MASH (77). JAK-STAT3 signaling induces IFNγ expression, which drives liver natural killer cell apoptosis during MASH that increases the production of Th-1 cytokines like TNF, IL-2, and IL-12, further exacerbating metainflammation (78, 79). STAT3 can also be activated by IL-6 signaling during liver inflammation (80). Mice that lack IL-6 are not completely protected from developing MASLD but exhibit a generally reduced inflammatory response to a steatotic diet (36).

The impact of STAT5 signaling on the development of MASLD/MASH is multifaceted. Studies have demonstrated a direct interaction between STAT5 and mTORC1 activity, contributing to *de novo* lipogenesis, MASH, and hepatocellular carcinoma (81). Conversely, JAK2-STAT5 signaling has been reported to play a protective role in the progression of MASH (Vesting, 2022 #1306), although JAK2 itself is implicated in advancing HCC (82). It has also been shown that STAT5 activation by IL-21 is necessary for Hodgkin lymphomagenesis (83).

In murine models lacking hepatic STAT5, MASLD is observed without evidence of hepatic inflammation or fibrosis (82); however, these animals exhibit an increased risk for developing HCC (84). In our studies, loss of the IL-21R did not abolish pSTAT5 levels but attenuated them to those seen in chow-fed *IL21R*$^{+/+}$ and *il21r*$^{-/-}$ mice, suggesting that precise regulation of STAT5 is essential for maintaining liver health.

There is a recent study that found that streptozotocin-treated *IL21R*$^{+/+}$ mice on a high fat diet developed MASH-associated HCC. Streptozotocin induces type 1 diabetes in mice by destroying β-cells, and the STAM model is commonly used to study MASH (85). Typically, these mice do not exhibit obesity, in contrast to humans with MASH, where obesity is considered a major contributing factor and the method we

used to produce MASLD/MASH (86). Another approach involved using a western style diet (21.2% fat; 41% sucrose; 1.25% cholesterol) combined with high fructose water (23.1 g/L) and weekly intraperitoneal CCl_4 injections (0.2 ml/g body weight) to induce liver fibrosis. Under these conditions, *Il21r*$^{-/-}$ mice demonstrated increased resistance to developing HCC and showed reduced levels of pSTAT1, which led to decreased activation of cytotoxic T cells. In our diet-induced obesity model for MASLD/MASH, no up regulation of pSTAT1^{Ser727} was observed in any cohort fed either diet.

It is well established that the liver of individuals with MASH experience hypoxic conditions (27). Hypoxia-induced factors play a significant role in promoting both fibrosis and the progression of MASH (31). Increased HIF-2α expression has been observed in the liver of mice subjected to hypoxic environments (58). Substantial evidence indicates that HIF-2α is critically involved in MASH progression by facilitating lipid accumulation (55, 56, 87). Studies have demonstrated that HIF-2α is a direct target of STAT5 activity in hematopoietic stem cells (57).

Our findings demonstrate that expression of the amino acid transporter SLC27A5 was increased in tissues with elevated HIF-2α levels (62). Mammalian target of rapamycin (mTOR) is known to respond to changes in amino acid concentrations (63). Amino acid influx appears to be the primary activator of mTOR activity. Activation of mTOR stimulates anabolic pathways essential for initiating and sustaining cell growth (61). Previous studies have indicated that mTOR promotes *de novo* lipogenesis *via* SREBP-dependent regulation of fatty acid and cholesterol gene expression (88). Thus IL-21R-induced expression of HIF-2α additionally drives mTOR-dependent lipogenesis, highlighting its significance as a downstream pathway activated by IL-21R signaling (62).

Conclusion

The findings demonstrate that activation of STAT5 through IL-21 receptor signaling promotes HIF-2α expression under hypoxic conditions in liver affected by MASH. The induction of HIF-2α enhances the transcription of genes associated with *de novo* lipogenesis. Additionally, HIF-2α facilitates further lipogenic activity by indirectly activating mTOR *via* increased *SLC27A5* expression, which supports amino acid uptake and initiates mTOR-dependent anabolic signaling. Notably, abrogation of IL-21 signaling through the deletion of IL-21R markedly attenuates MASLD/MASH.

Our ongoing research is aimed at clarifying how IL-21, JAK-STAT5 signaling, and MASH are related. It will also be necessary to demonstrate a direct interaction between pSTAT5 and the HIF-2α promoter *in vivo* during MASH. *in vivo* shRNA knockdown studies of JAK1, STAT3, and STAT5 will be needed to define their roles in MASH through IL-21R signaling, and a direct JAK1-STAT5 interaction must be established. Additional cell culture experiments with phosphorylation mutants may yield *in vitro* data relevant for future mechanistic studies. Additionally, to definitively determine how IL-21R influences lipogenesis triggered by a high-fat diet, *in vivo* studies that specifically measure *de novo* lipogenesis are necessary.

Experimental procedures

Miscellaneous reagents

Chemicals, proteinase inhibitor-phosphatase inhibitor cocktail (#7834), nuclease (#88701), and collagenase (#C3867) were obtained from Millipore Sigma. SDS-PAGE and Western blot supplies were purchased from BIO-RAD. Histological staining reagents came from Agilent. Primers and master mix for *q*RT-PCR were acquired from Thermo Fisher Scientific.

HepG2 cell PA treatment assay

HepG2 cells were treated with 500 μM PA for 24 h as described (37).

Animal studies

Male *IL-21R*$^{+/+}$ (C57BL/6NJ) mice (n = 6) and *Il-21r*$^{-/-}$ (Jax B6.129-*IL-21*^{rtm1Kopf}/J homozygous) mice (n = 10), each 6 weeks old, were used for all studies. The animals were housed individually under a 12-h light/dark cycle. They were provided either standard chow (Picochow 5053, LabDiets, Richmond, VA) or a high fat diet (HFD; D12492i (60% fat), Research Diets, New Brunswick, NJ) and had water *ad libitum* for 16 weeks.

Animals were euthanized by CO_2-induced asphyxiation followed by cervical dislocation. Replacement, Reduction, and Refinement principles were used, and procedures were implemented to minimize any suffering and distress for the ethical and humane treatment of animals. The Invivotek IACUC approved all studies following procedures according to the "*Institutional Animal Care and Use Committee Handbook*".

Oral glucose tolerance test

Mice fasted for 16 h before the study. Blood glucose was checked at baseline, and at 15, 30, 60, and 120 min after administering 2 g/kg glucose (100 mg/ml) *via* oral gavage. Glucose levels were assessed with a One-touch Ultra 2 glucometer, and insulin with an electrochemiluminescence kit (MA2400 Mouse/Rat insulin kit K152BZC, Meso Scale Discovery).

Insulin tolerance test

Mice fasted for 4 h before the study. Baseline insulin was measured from a tail tip sample. Chow-fed mice received 0.5 units/kg insulin intraperitoneally; HFD mice received 1.0 units/kg. Blood glucose was checked at 15, 30, 60, and 90 min.

Serum clinical chemistries

Serum samples were obtained and subsequently analyzed with the ACE Alera system (Alfa Wasserman), following the manufacturer's protocol.

Lipid extraction from mouse tissues

Liver tissue (100 mg) was homogenized and extracted using hexane:2-propanol (3:2). Samples were centrifuged, transferred to glass tubes, and washed with 0.9% NaCl. Following centrifugation, the aqueous phase was removed, while the organic phase was dried and stored in isopropyl alcohol until analysis. Triglyceride and cholesterol concentrations were measured using the Cayman Triglyceride Colorimetric Assay kit and the Promega Cholesterol/Cholesterol Ester GloTM assay kit, respectively.

H&E and trichrome C histological staining protocol

The left lobes of several liver were stored in 10% neutral buffered saline for histology staining. The tissues were embedded in parafilm and sectioned at 5 mm thickness. Sections were then mounted on slides, subjected to multiple rounds of ethanol dehydration, and delipidated. Liver sections were stained with hematoxylin (Leica Biosystems) and eosin (Leica Biosystems), or trichrome C (Polyscience Inc.).

Protein extraction

Tissue samples were homogenized in RIPA buffer containing phosphatase and protease inhibitors. Cell lysates were collected through low-speed centrifugation and stored at −20 °C until further analysis. Protein concentrations were measured using the Pierce BCA Protein Assay Kit.

Western blotting

Cell lysates containing 25 μg of protein were resuspended in sample buffer and separated by SDS-PAGE. After transfer to nitrocellulose, membranes were incubated with TBST (Tris-buffered saline, 0.1% Tween 20) containing 10% milk for 1 h to overnight.

Membranes were washed several times with TBST, and then incubated with primary antibodies for 12 to 16 h. This was followed by additional washes and incubation with secondary antibodies for 1 to 4 h. Following further washes with TBST, membranes were treated with a chemiluminescent agent (Cytiva, Amersham ECL Prime Western Blotting Detection Reagent). Protein detection was performed using an Amersham Imager 600. GAPDH was used as the loading control for all Western blot analyses. Antibodies used are listed in Table S1.

For densitometry analysis, TIFF images of western blots were adjusted to 150 brightness using the Image tab/adjustments/brightness function in Adobe Photoshop (version 26.1.0) to establish a normalized baseline.

Protein microarray analysis

The Mouse JAK/STAT Pathway Phosphorylation Array C1 (RayBiotech) was used to measure the protein levels of various JAK-STAT proteins following the manufacturer's instructions.

ELISA assays

ELISA assays followed the manufacturer's protocol using lysates from blood or liver tissue. ELISA kits used are listed in Table S2.

Cell based TGF-β1 protein assay

Total and active TGFβ levels were quantified *via* a cell-based assay, conducted according to established protocols, using a commercial kit (BPS Bioscience, Cat# 60544).

RNA isolation

Total RNA was extracted from liver tissue using the RNeasy Mini kit (Qiagen) in accordance with the manufacturer's instructions. A Bullet Blender 24 Gold (Next Advance) was employed to homogenize murine liver tissue in RLT lysis buffer. Ethyl alcohol (200-proof, Pharmco by Greenfield Global) was subsequently added, and samples were loaded onto an RNeasy column. The RNA underwent washing with RW1 buffer and on-column DNase digestion utilizing a RNase-Free DNase Set (Qiagen). Additional washes were performed with RNeasy RW1 and RPE buffers. Total RNA was eluted in RNase-free water, measured *via* a NanoDrop ND-1000 spectrophotometer (Thermo Fisher Scientific), and stored at −80 °C.

Quantitative revereverse transcription-polymerase chain reaction analysis

Total RNA was reverse transcribed utilizing the QuantiTect Reverse Transcription kit (Qiagen), followed by PCR amplification with the Power SYBR RNA-to-CT 1-Step Kit (Thermo Fisher Scientific). GAPDH expression served as an internal control.

Immunohistochemistry protocol

Liver histology slides (USBioMax LV1201 B; IL-21R staining) (Novus Biologics, #NBP230274; NBP2-30273; co-localization staining) were deparaffinized and rehydrated with xylene and ethanol, then rinsed in distilled water. IL-21R antigen retrieval was performed by heating slides in Tris-HCl-EDTA buffer (pH 9.0) at 95 to 100 °C for 20 min, cooling to room temperature, and rinsing with PBS. Endogenous peroxidase was blocked by incubating slides in 3% H_2O_2 in PBS for 10 min at room temperature. The slides were blocked with 5 to 10% normal goat serum for 30 min. IL-21R protein was detected using anti-IL-21R antibodies (1:250, Bioss Inc, Woburn, MA) and anti-CD4 antibody (1:200, Sino Biological Inc, Paoli, PA) in PBS with 1% BSA overnight at 4 °C. Slides were washed with PBS, and then incubated with secondary antibody ABC kits and DAB reagents.

Statistical analysis

in vivo data were analyzed using two-way ANOVA with Dunnett's *post hoc* test compared to chow-fed mice. Data are presented as mean ± SD. All other datasets were evaluated using two-way ANOVA with Tukey's *post hoc* analysis unless

otherwise indicated in the figure legend. Results are reported as mean ± SD.

Data availability

All data is available upon request.

Supporting information—This article contains supporting information.

Acknowledgments—Invivotek, L. L. C. conducted all *in vivo* experiments under the supervision of Dr Michael Hayward and Ms Caroline Giordano. The members of the Institute of Metabolic Disorders and Invivotek provided guidance during the *in vivo* studies. Discussions with Drs. Martin Adelson and Eli Mordechai contributed to the research.

Author contributions—K. K. F. and J. T. N. supervision; K. K. F. and J. T. N. methodology; K. K. F., A. B., D. D., R. F., P. J., and J. T. N. investigation; K. K. F., A. B., D. D., R. F., P. J., and J. T. N. formal analysis; K. K. F. data curation; K. K. F. and J. T. N. conceptualization; A. B., D. D., R. F., P. J., and J. T. N. validation; J. T. N. writing–review and editing; J. T. N. writing-original draft.

Funding and additional information—This research was supported by funding from Genesis Biotechnology Group, Inc.

Conflict of interest—The authors declare that they have no conflicts of interest with the contents of this article.

Abbreviations—The abbreviations used are: αSMA, a smooth muscle actin; ALP, alkaline phosphatase; AST, aspartate aminotransferase; COL1A1, collagen 1α 1 chain; HIF-2α, hypoxia-induced factor 2 alpha; HFD, high-fat diet; IL-21, interleukin-21; IL-21R, interleukin-21 receptor; HSC, hepatic stellate cell; JAK, Janus kinase; MASH, metabolic dysfunction-associated steatohepatitis; MASLD, metabolic dysfunction-associated steatotic liver disease; mTOR, mammalian target of rapamycin; PA, palmitic acid; RIG-I, retinoic acid-inducible gene I; SLC7A5, solute carrier family 7 member 5; *TNFRSF9*, tumor necrosis family receptor super family 9.

References

1. Tincopa, M. A., Anstee, Q. M., and Loomba, R. (2024) New and emerging treatments for metabolic dysfunction-associated steatohepatitis. *Cell Metab.* **36**, 912–926
2. Polyzos, S. A., Kountouras, J., and Mantzoros, C. S. (2019) Obesity and nonalcoholic fatty liver disease: from pathophysiology to therapeutics. *Metabolism* **92**, 82–97
3. Koliaki, C., Dalamaga, M., and Liatis, S. (2023) Update on the obesity epidemic: after the sudden rise, is the upward trajectory beginning to flatten? *Curr. Obes. Rep.* **12**, 514–527
4. Allen, A. M., Lazarus, J. V., and Younossi, Z. M. (2023) Healthcare and socioeconomic costs of NAFLD: a global framework to navigate the uncertainties. *J. Hepatol.* **79**, 209–217
5. Keam, S. J. (2024) Resmetirom: first approval. *Drugs* **84**, 729–735
6. Tiwari, A., Sharma, A., Kumar, H., Gupta, V., Deshpande, V., Muppaaju, J. S., *et al.* (2025) Resmetirom for MASH: a comprehensive review of a novel therapeutic frontier. *Biomedicines* **13**, 2079
7. Wegovy approved for MASH. *Nat. Biotechnol.* **43**, (2025), 1404
8. Ismaiel, A., Scarlata, G. G. M., Boitos, I., Leucuta, D. C., Popa, S. L., Al Srouji, N., *et al.* (2025) Gastrointestinal adverse events associated with GLP-1 RA in non-diabetic patients with overweight or obesity: a systematic review and network meta-analysis. *Int. J. Obes. (Lond)* **49**, 1946–1957
9. Filippatos, T. D., Panagiotopoulou, T. V., and Elisaf, M. S. (2014) Adverse effects of GLP-1 receptor agonists. *Rev. Diabet Stud.* **11**, 202–230
10. Coutinho, W., and Halpern, B. (2024) Pharmacotherapy for obesity: moving towards efficacy improvement. *Diabetol. Metab. Syndr.* **16**, 6
11. Leonard, W. J., and Wan, C. K. (2016) IL-21 signaling in immunity. *F1000Res* **5**
12. Tangye, S. G. (2015) Advances in IL-21 biology - enhancing our understanding of human disease. *Curr. Opin. Immunol.* **34**, 107–115
13. Spolski, R., and Leonard, W. J. (2014) Interleukin-21: a double-edged sword with therapeutic potential. *Nat. Rev. Drug Discov.* **13**, 379–395
14. Zeng, R., Spolski, R., Casas, E., Zhu, W., Levy, D. E., and Leonard, W. J. (2007) The molecular basis of IL-21-mediated proliferation. *Blood* **109**, 4135–4142
15. Spolski, R., and Leonard, W. J. (2008) Interleukin-21: basic biology and implications for cancer and autoimmunity. *Annu. Rev. Immunol.* **26**, 57–79
16. Hu, X., Li, J., Fu, M., Zhao, X., and Wang, W. (2021) The JAK/STAT signaling pathway: from bench to clinic. *Signal Transduct Target Ther.* **6**, 402
17. Xie, Y., Huang, Y., Li, Z. Y., Jiang, W., Shi, N. X., Lu, Y., *et al.* (2024) Interleukin-21 receptor signaling promotes metabolic dysfunction-associated steatohepatitis-driven hepatocellular carcinoma by inducing immunosuppressive IgA(+) B cells. *Mol. Cancer* **23**, 95
18. Yang, X., Liao, L., Liang, Z., Yu, S., and Guo, Z. (2024) Correlation analysis of IL-17, IL-21, IL-23 with non-alcoholic liver fibrosis and cirrhosis. *J. Inflamm. Res.* **17**, 2327–2335
19. Zhang, Z., Wang, J., Li, H., Niu, Q., Tao, Y., Zhao, X., *et al.* (2025) The role of the interleukin family in liver fibrosis. *Front Immunol.* **16**, 1497095
20. Xu, Y. F., Yao, Y., Ma, M., Yang, S. H., Jiang, P., Wang, J., *et al.* (2022) The proinflammatory cytokines IL-18, IL-21, and IFN-gamma differentially regulate liver inflammation and anti-mitochondrial antibody level in a murine model of primary biliary cholangitis. *J. Immunol. Res.* **2022**, 7111445
21. Pesce, J., Kaviratne, M., Ramalingam, T. R., Thompson, R. W., Urban, J. F., Jr., Cheever, A. W., *et al.* (2006) The IL-21 receptor augments Th2 effector function and alternative macrophage activation. *J. Clin. Invest.* **116**, 2044–2055
22. Li, J., Chen, Q., Yi, J., Lan, X., Lu, K., Du, X., *et al.* (2021) IFN-gamma contributes to the hepatic inflammation in HFD-induced nonalcoholic steatohepatitis by STAT1beta/TLR2 signaling pathway. *Mol. Immunol.* **134**, 118–128
23. Feng, G., Zhang, J. Y., Zeng, Q. L., Yu, X., Zhang, Z., Lv, S., *et al.* (2014) Interleukin-21 mediates hepatitis B virus-associated liver cirrhosis by activating hepatic stellate cells. *Hepatol. Res.* **44**, E198–E205
24. Friedman, S. L., Neuschwander-Tetri, B. A., Rinella, M., and Sanyal, A. J. (2018) Mechanisms of NAFLD development and therapeutic strategies. *Nat. Med.* **24**, 908–922
25. Musso, G., Cassader, M., Olivetti, C., Rosina, F., Carbone, G., and Gambino, R. (2013) Association of obstructive sleep apnoea with the presence and severity of non-alcoholic fatty liver disease. A systematic review and meta-analysis. *Obes. Rev.* **14**, 417–431
26. Borel, A. L. (2019) Sleep apnea and sleep habits: relationships with metabolic syndrome. *Nutrients* **11**, 2628
27. Isaza, S. C., Del Pozo-Maroto, E., Dominguez-Alcon, L., Elbouayadi, L., Gonzalez-Rodriguez, A., and Garcia-Monzon, C. (2020) Hypoxia and non-alcoholic fatty liver disease. *Front Med. (Lausanne)* **7**, 578001
28. Li, J., Grigoryev, D. N., Ye, S. Q., Thorne, L., Schwartz, A. R., Smith, P. L., *et al.* (2005) Chronic intermittent hypoxia upregulates genes of lipid biosynthesis in obese mice. *J. Appl. Physiol. (1985)* **99**, 1643–1648
29. Chen, J., Chen, J., Fu, H., Li, Y., Wang, L., Luo, S., *et al.* (2019) Hypoxia exacerbates nonalcoholic fatty liver disease via the HIF-2alpha/PPARalpha pathway. *Am. J. Physiol. Endocrinol. Metab.* **317**, E710–E722
30. Fu, Y., Zhang, N., Tang, W., Bi, Y., Zhu, D., Chu, X., *et al.* (2022) Chronic intermittent hypoxia contributes to non-alcoholic steatohepatitis progression in patients with obesity. *Hepatol. Int.* **16**, 824–834

31. Cai, H., Bai, Z., and Ge, R. L. (2021) Hypoxia-inducible factor-2 promotes liver fibrosis in non-alcoholic steatohepatitis liver disease via the NF-kappaB signalling pathway. *Biochem. Biophys. Res. Commun.* **540**, 67–74
32. Holzner, L. M. W., and Murray, A. J. (2021) Hypoxia-Inducible factors as key players in the pathogenesis of non-alcoholic fatty liver disease and non-alcoholic steatohepatitis. *Front Med. (Lausanne)* **8**, 753268
33. Wang, T., Cunningham, A., Dokun, A. O., Hazarika, S., Houston, K., Chen, L., *et al.* (2015) Loss of interleukin-21 receptor activation in hypoxic endothelial cells impairs perfusion recovery after hindlimb ischemia. *Arterioscler Thromb. Vasc. Biol.* **35**, 1218–1225
34. Cai, J., Hu, M., Chen, Z., and Ling, Z. (2021) The roles and mechanisms of hypoxia in liver fibrosis. *J. Transl. Med.* **19**, 186
35. Tomita, K., Tamiya, G., Ando, S., Ohsumi, K., Chiyo, T., Mizutani, A., *et al.* (2006) Tumour necrosis factor alpha signalling through activation of Kupffer cells plays an essential role in liver fibrosis of non-alcoholic steatohepatitis in mice. *Gut* **55**, 415–424
36. Mas, E., Danjoux, M., Garcia, V., Carpentier, S., Segui, B., and Levade, T. (2009) IL-6 deficiency attenuates murine diet-induced non-alcoholic steatohepatitis. *PLoS One* **4**, e7929
37. Frietze, K. K., Brown, A. M., Das, D., Franks, R. G., Cunningham, J. L., Hayward, M., *et al.* (2022) Lipotoxicity reduces DDX58/Rig-1 expression and activity leading to impaired autophagy and cell death. *Autophagy* **18**, 142–160
38. Willy, J. A., Young, S. K., Stevens, J. L., Masuoka, H. C., and Wek, R. C. (2015) CHOP links endoplasmic reticulum stress to NF-kappaB activation in the pathogenesis of nonalcoholic steatohepatitis. *Mol. Biol. Cell* **26**, 2190–2204
39. Zimmermann, H. W., Seidler, S., Gassler, N., Nattermann, J., Luedde, T., Trautwein, C., *et al.* (2011) Interleukin-8 is activated in patients with chronic liver diseases and associated with hepatic macrophage accumulation in human liver fibrosis. *PLoS One* **6**, e21381
40. Dostert, C., Grusdat, M., Letellier, E., and Brenner, D. (2019) The TNF family of ligands and receptors: communication modules in the immune system and beyond. *Physiol. Rev.* **99**, 115–160
41. Wu, X., Song, Y., and Wu, S. (2024) Relation of 91 circulating inflammatory proteins to nonalcoholic fatty liver disease: a two-sample mendelian randomisation study. *J. Cell Mol. Med.* **28**, e70322
42. Colella, F., Henderson, N. C., and Ramachandran, P. (2025) Dissecting the mechanisms of MASLD fibrosis in the era of single-cell and spatial omics. *J. Clin. Invest.* **135**, e186421
43. Xing, J., Guan, X., Zhang, Q., Chen, S., Wu, S., and Sun, X. (2021) Triglycerides mediate body mass index and nonalcoholic fatty liver disease: a population-based study. *Obes. Facts* **14**, 190–196
44. Sattar, N., Forrest, E., and Preiss, D. (2014) Non-alcoholic fatty liver disease. *BMJ* **349**, g4596
45. Stein, W., Bohner, J., Renn, W., and Maulbetsch, R. (1985) Macro creatine kinase type 2: results of a prospective study in hospitalized patients. *Clin. Chem.* **31**, 1959–1964
46. Meffert, G., Gellerich, F. N., Margreiter, R., and Wyss, M. (2005) Elevated creatine kinase activity in primary hepatocellular carcinoma. *BMC Gastroenterol.* **5**, 9
47. He, Y., Chen, Y., Qian, S., van Der Merwe, S., Dhar, D., Brenner, D. A., *et al.* (2025) Immunopathogenic mechanisms and immunoregulatory therapies in MASLD *Cell. Mol. Immunol.* **22**, 1159–1177
48. Tsuchida, T., and Friedman, S. L. (2017) Mechanisms of hepatic stellate cell activation. *Nat. Rev. Gastroenterol. Hepatol.* **14**, 397–411
49. Wiering, L., Subramanian, P., and Hammerich, L. (2023) Hepatic Stellate cells: dictating outcome in nonalcoholic fatty liver disease. *Cell. Mol. Gastroenterol. Hepatol.* **15**, 1277–1292
50. Wang, P. W., Wu, T. H., Lin, T. Y., Chen, M. H., Yeh, C. T., and Pan, T. L. (2019) Characterization of the roles of vimentin in regulating the proliferation and migration of HSCs during hepatic fibrogenesis. *Cells* **8**, 1184
51. Hellerbrand, C., Stefanovic, B., Giordano, F., Burchardt, E. R., and Brenner, D. A. (1999) The role of TGFbeta1 in initiating hepatic stellate cell activation in vivo. *J. Hepatol.* **30**, 77–87
52. Deng, Z., Fan, T., Xiao, C., Tian, H., Zheng, Y., Li, C., *et al.* (2024) TGF-beta signaling in health, disease, and therapeutics. *Signal Transduct. Target Ther.* **9**, 61
53. Lorenz, U. (2009) SHP-1 and SHP-2 in T cells: two phosphatases functioning at many levels. *Immunol. Rev.* **228**, 342–359
54. Jones, M. L., Craik, J. D., Gibbins, J. M., and Poole, A. W. (2004) Regulation of SHP-1 tyrosine phosphatase in human platelets by serine phosphorylation at its C terminus. *J. Biol. Chem.* **279**, 40475–40483
55. Qu, A., Taylor, M., Xue, X., Matsubara, T., Metzger, D., Chambon, P., *et al.* (2011) Hypoxia-inducible transcription factor 2alpha promotes steatohepatitis through augmenting lipid accumulation, inflammation, and fibrosis. *Hepatology* **54**, 472–483
56. Gonzalez, F. J., Xie, C., and Jiang, C. (2018) The role of hypoxia-inducible factors in metabolic diseases. *Nat. Rev. Endocrinol.* **15**, 21–32
57. Fatrai, S., Wierenga, A. T., Daenen, S. M., Vellenga, E., and Schuringa, J. J. (2011) Identification of HIF2alpha as an important STAT5 target gene in human hematopoietic stem cells. *Blood* **117**, 3320–3330
58. Cao, R., Zhao, X., Li, S., Zhou, H., Chen, W., Ren, L., *et al.* (2014) Hypoxia induces dysregulation of lipid metabolism in HepG2 cells via activation of HIF-2alpha. *Cell. Physiol. Biochem.* **34**, 1427–1441
59. Chen, M., Zhang, J., Sampieri, K., Clohessy, J. G., Mendez, L., Gonzalez-Billalabeitia, E., *et al.* (2018) An aberrant SREBP-dependent lipogenic program promotes metastatic prostate cancer. *Nat. Genet.* **50**, 206–218
60. Saxton, R. A., and Sabatini, D. M. (2017) mTOR signaling in growth, metabolism, and disease. *Cell* **168**, 960–976
61. Panwar, V., Singh, A., Bhatt, M., Tonk, R. K., Azizov, S., Raza, A. S., *et al.* (2023) Multifaceted role of mTOR (mammalian target of rapamycin) signaling pathway in human health and disease. *Signal Transduct. Target Ther.* **8**, 375
62. Elorza, A., Soro-Arnaiz, I., Melendez-Rodriguez, F., Rodriguez-Vaello, V., Marsboom, G., de Carcer, G., *et al.* (2012) HIF2alpha acts as an mTORC1 activator through the amino acid carrier SLC7A5. *Mol. Cell* **48**, 681–691
63. Kim, Y. C., and Guan, K. L. (2015) mTOR: a pharmacologic target for autophagy regulation. *J. Clin. Invest.* **125**, 25–32
64. Kageyama, S., Gudmundsson, S. R., Sou, Y. S., Ichimura, Y., Tamura, N., Kazuno, S., *et al.* (2021) p62/SQSTM1-droplet serves as a platform for autophagosome formation and anti-oxidative stress response. *Nat. Commun.* **12**, 16
65. Fukushima, H., Yamashina, S., Arakawa, A., Taniguchi, G., Aoyama, T., Uchiyama, A., *et al.* (2018) Formation of p62-positive inclusion body is associated with macrophage polarization in non-alcoholic fatty liver disease. *Hepatol. Res.* **48**, 757–767
66. Zhang, C., Huang, C., Xia, H., Xu, H., Tang, Q., and Bi, F. (2022) Autophagic sequestration of SQSTM1 disrupts the aggresome formation of ubiquitinated proteins during proteasome inhibition. *Cell Death Dis.* **13**, 615
67. Klionsky, D. J., Baehrecke, E. H., Brumell, J. H., Chu, C. T., Codogno, P., Cuervo, A. M., *et al.* (2011) A comprehensive glossary of autophagy-related molecules and processes. *Autophagy* **7**, 1273–1294
68. Kabeya, Y., Mizushima, N., Ueno, T., Yamamoto, A., Kirisako, T., Noda, T., *et al.* (2000) LC3, a mammalian homologue of yeast Apg8p, is localized in autophagosome membranes after processing. *EMBO J.* **19**, 5720–5728
69. Petroski, M. D., and Deshaies, R. J. (2005) Mechanism of lysine 48-linked ubiquitin-chain synthesis by the cullin-RING ubiquitin-ligase complex SCF-Cdc34. *Cell* **123**, 1107–1120
70. Tian, Y., and Zajac, A. J. (2016) IL-21 and T cell differentiation: consider the context. *Trends Immunol.* **37**, 557–568
71. Sun, L., Su, Y., Jiao, A., Wang, X., and Zhang, B. (2023) T cells in health and disease. *Signal Transduct. Target Ther.* **8**, 235
72. Corbit, K. C., Camporez, J. P. G., Tran, J. L., Wilson, C. G., Lowe, D. A., Nordstrom, S. M., *et al.* (2017) Adipocyte JAK2 mediates growth hormone-induced hepatic insulin resistance. *JCI Insight.* **2**, e91001
73. Corbit, K. C., Wilson, C. G., Lowe, D., Tran, J. L., Vera, N. B., Clasquin, M., *et al.* (2019) Adipocyte JAK2 mediates spontaneous

metabolic liver disease and hepatocellular carcinoma. *JCI Insight* **5**, e131310
74. Rochman, Y., Kashyap, M., Robinson, G. W., Sakamoto, K., Gomez-Rodriguez, J., Wagner, K. U., *et al.* (2010) Thymic stromal lymphopoietin-mediated STAT5 phosphorylation via kinases JAK1 and JAK2 reveals a key difference from IL-7-induced signaling. *Proc. Natl. Acad. Sci. U. S. A.* **107**, 19455–19460
75. Liu, K. D., Gaffen, S. L., Goldsmith, M. A., and Greene, W. C. (1997) Janus kinases in interleukin-2-mediated signaling: JAK1 and JAK3 are differentially regulated by tyrosine phosphorylation. *Curr. Biol.* **7**, 817–826
76. Song, Z., Liu, X., Zhang, W., Luo, Y., Xiao, H., Liu, Y., *et al.* (2022) Ruxolitinib suppresses liver fibrosis progression and accelerates fibrosis reversal via selectively targeting Janus kinase 1/2. *J. Transl. Med.* **20**, 157
77. Jung, K. H., Yoo, W., Stevenson, H. L., Deshpande, D., Shen, H., Gagea, M., *et al.* (2017) Multifunctional effects of a small-molecule STAT3 inhibitor on NASH and hepatocellular carcinoma in mice. *Clin. Cancer Res.* **23**, 5537–5546
78. Brenner, C., Galluzzi, L., Kepp, O., and Kroemer, G. (2013) Decoding cell death signals in liver inflammation. *J. Hepatol.* **59**, 583–594
79. Deng, Z. B., Liu, Y., Liu, C., Xiang, X., Wang, J., Cheng, Z., *et al.* (2009) Immature myeloid cells induced by a high-fat diet contribute to liver inflammation. *Hepatology* **50**, 1412–1420
80. He, G., and Karin, M. (2011) NF-kappaB and STAT3 - key players in liver inflammation and cancer. *Cell Res.* **21**, 159–168
81. Li, T., Weng, J., Zhang, Y., Liang, K., Fu, G., Li, Y., *et al.* (2019) mTOR direct crosstalk with STAT5 promotes de novo lipid synthesis and induces hepatocellular carcinoma. *Cell Death Dis.* **10**, 619
82. Kaltenecker, D., Themanns, M., Mueller, K. M., Spirk, K., Suske, T., Merkel, O., *et al.* (2019) Hepatic growth hormone - JAK2 - STAT5 signalling: Metabolic function, non-alcoholic fatty liver disease and hepatocellular carcinoma progression. *Cytokine* **124**, 154569
83. Scheeren, F. A., Diehl, S. A., Smit, L. A., Beaumont, T., Naspetti, M., Bende, R. J., *et al.* (2008) IL-21 is expressed in Hodgkin lymphoma and activates STAT5: evidence that activated STAT5 is required for Hodgkin lymphomagenesis. *Blood* **111**, 4706–4715
84. Mueller, K. M., Kornfeld, J. W., Friedbichler, K., Blaas, L., Egger, G., Esterbauer, H., *et al.* (2011) Impairment of hepatic growth hormone and glucocorticoid receptor signaling causes steatosis and hepatocellular carcinoma in mice. *Hepatology* **54**, 1398–1409
85. Wu, J. (2016) Utilization of animal models to investigate nonalcoholic steatohepatitis-associated hepatocellular carcinoma. *Oncotarget* **7**, 42762–42776
86. Gallage, S., Avila, J. E. B., Ramadori, P., Focaccia, E., Rahbari, M., Ali, A., *et al.* (2022) A researcher's guide to preclinical mouse NASH models. *Nat. Metab.* **4**, 1632–1649
87. Chu, Q., Gu, X., Zheng, Q., and Zhu, H. (2022) Regulatory mechanism of HIF-1alpha and its role in liver diseases: a narrative review. *Ann. Transl Med.* **10**, 109
88. Eid, W., Dauner, K., Courtney, K. C., Gagnon, A., Parks, R. J., Sorisky, A., *et al.* (2017) mTORC1 activates SREBP-2 by suppressing cholesterol trafficking to lysosomes in mammalian cells. *Proc. Natl. Acad. Sci. U. S. A.* **114**, 7999–8004
89. Crowe, A. R., and Yue, W. (2019) Semi-quantitative determination of protein expression using immunohistochemistry staining and analysis: an integrated protocol. *Bio Protoc.* **9**, e3465